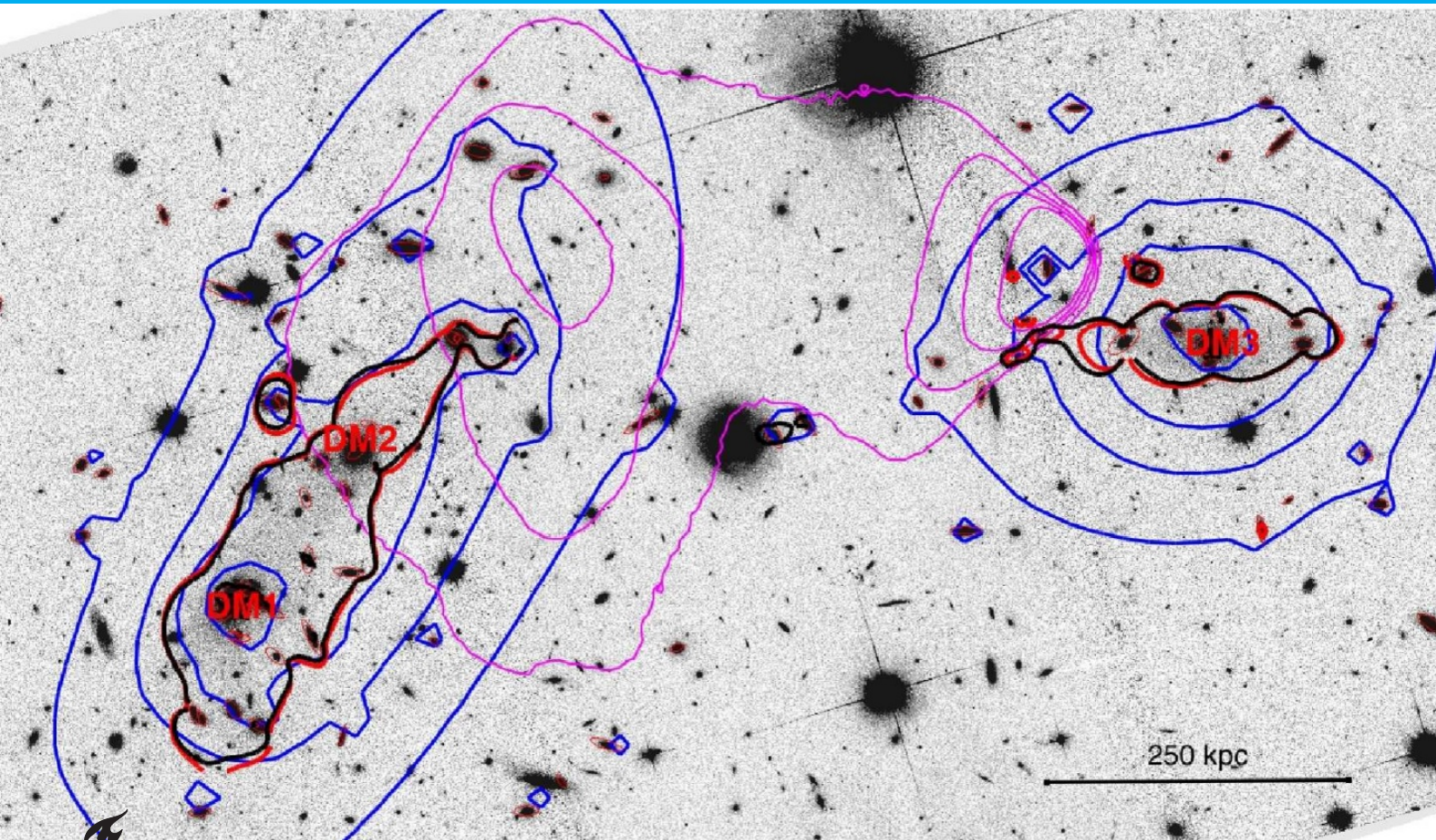


Modified Newtonian Dynamics and the Bullet Cluster

A comparison with the dark
matter model

Darwin Liu

Bachelor endproject 2022



Modified Newtonian Dynamics and the Bullet Cluster

A comparison with the dark matter model

by

Darwin Liu

to obtain the degree of Bachelor of Science
at the Delft University of Technology,
to be defended publicly on Tuesday July 12, 2022 at 2:00 PM.

Student number:	5171695
Project duration:	February 12, 2022 – July 12, 2022
Thesis committee:	Dr. P.M. Visser, TU Delft, supervisor
	Dr. S.W.H. Eijt, TU Delft, supervisor
	Dr. A.R. Akhmerov, TU Delft
	W.G.M. Groenevelt, TU Delft

An electronic version of this thesis is available at <http://repository.tudelft.nl/>.

Contents

1	Introduction	3
2	Newtonian gravitational potential	7
2.1	Potential of point masses	7
2.2	The Poisson equation	8
2.3	Shell theorem	8
2.4	Velocity of orbitals	9
3	MOND	11
3.1	The MOND equations	11
3.2	Verlinde interpolation	12
3.3	Other interpolation functions	13
4	Bullet Cluster	17
5	Generation of the model and numerical solutions	19
5.1	Modelling a Bullet cluster-like cluster	19
5.1.1	Discretization of volume of space	19
5.1.2	Generation of the mass distribution	19
5.2	Solving ND Numerically	21
5.2.1	Fourier transform	21
5.2.2	Fast Fourier Transform	22
5.2.3	Analytic calculation vs numerical approximation of 2 point masses	22
5.3	Helmholtz decomposition with Fourier transform	23
5.4	Solving MOND Numerically	23
5.4.1	Inverse interpolation function	24
5.4.2	The iterative method	24
5.5	Apparent mass distribution and apparent dark matter distribution	25
6	Comparison between ND and MOND on a Bullet-like cluster	27
6.1	Mass distribution of a Bullet-like cluster and Newtonian gravity	27
6.2	Using MOND on the Bullet-like cluster	31
6.2.1	Standard interpolation	31
6.2.2	MOND with Angus interpolation	35
6.3	Changing the mass of the galaxies	39
6.4	Changing the number of the galaxies	41
7	Discussion of the results	43
8	Conclusions and recommendations for further research	45
	Bibliography	47
A	MOND with the Verlinde interpolation function	49
B	Code	53

Abstract

The Bullet Cluster is a galaxy cluster, which is often used as evidence for dark matter [10]. In this thesis, Modified Newtonian Dynamics (MOND) is studied for various interpolation functions on a model of the Bullet Cluster. MOND is a theory proposed by Milgrom which modifies the Newtonian gravity law, such that it explains the flat rotation curves observed in all the galaxies and galaxy clusters [13]. It is an alternative theory to the dark matter model and in this thesis, the results of MOND are compared to results from the paper of Paraficz et al which have studied the Bullet Cluster with the dark matter model [15]. In MOND, the Newtonian gravity law is changed at low accelerations, for a around and below the value of $1.2 \cdot 10^{-10} \text{ m/s}^2$, which is introduced as a constant a_0 by Milgrom. Accelerations much smaller than a_0 are in the deep MOND regime and should satisfy certain conditions. Combining the low acceleration regime ($a \ll a_0$) and the Newton regime ($a \gg a_0$), an interpolation function is needed. The following interpolation functions are studied: the standard interpolation function, the Verlinde interpolation function and the Angus interpolation function.

First the Newtonian gravitational potential Φ_N is introduced which can be calculated for a certain mass distribution ρ using the Poisson equation. Also the acceleration field can be obtained from Φ_N . It could be seen that in the model used in this thesis for the Bullet Cluster, the strength of the acceleration field a is mostly below a_0 , but not much. Similarly the MOND potential Φ_M can also be calculated for ρ with the MOND equations, which are different equations for each interpolation function. The MOND equations are non-linear and can not be solved analytically in most cases. Thus a numerical iterative method is introduced to solve the MOND equations and to obtain Φ_M . After obtaining Φ_M for each interpolation function, the acceleration field f can also be calculated. We found that Φ_M is steeper than Φ_N for all interpolation functions. Also the acceleration field f is larger than a , and f is mostly above a_0 in the model of the Bullet Cluster used in this thesis.

By substituting Φ_M in the Poisson equation, another mass distribution could be obtained: apparent matter. This would be the matter distribution needed to give the acceleration field f using the Newtonian gravity law. From this matter distribution, the apparent dark matter could be obtained. We can compare this apparent dark matter distribution with the dark matter model found in the paper in Paraficz et al. Also the apparent matter distribution can be compared to the image of the Bullet Cluster. For both apparent dark matter and apparent matter, the MOND model is not in agreement with the dark matter model and the observation respectively. In general, the dark matter did not spatially coincide with the galaxies. By increasing the number of galaxies or increasing the mass of the galaxies, dark matter distributions that spatially coincide with the galaxies can be obtained.

1

Introduction

In the twentieth century, a lot more became known about our universe. But this also raised a lot of new questions. In 1933, Fritz Zwicky was studying the velocities at which galaxies were moving in galaxy clusters by observing the redshift of the light coming from these galaxies. The galaxies on the edge of the cluster were moving much faster than could be explained by visible matter according to Newtonian Dynamics (ND) [25]. To see this, it is useful to look at rotation curves. A rotation curve of a galaxy or galaxy cluster plots the velocity of the stars or galaxies respectively against their distance to the center. In figure 1.1, an example is given of a rotation curve of the galaxy NCD. What is remarkable is that the velocities of the galaxies become constant for larger distances: the flat rotation curve. This seems to be typical for rotation curves of clusters and galaxies [17]. ND, however, predicts that, assuming centrally concentrated mass, the rotation curve does not become constant, but will be approximately proportional to $\frac{1}{\sqrt{r}}$ for large distances, with r the distance to the center of the cluster. ND is thus inconsistent with the observations, as will be explained in more detail in section 2.

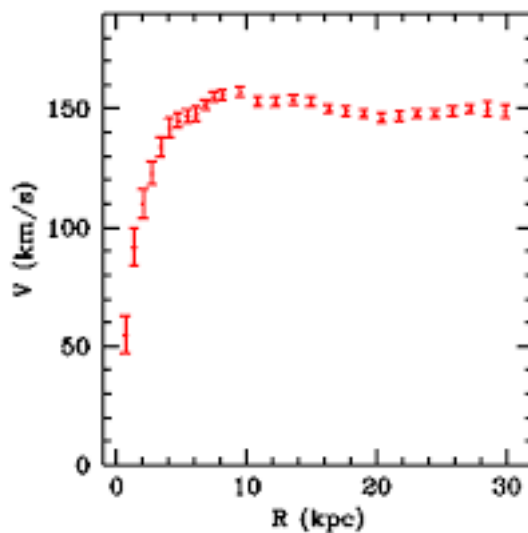


Figure 1.1: Rotation curve for the galaxy NGC3198 [5]. Here the y-axis is the velocity in km/s and the x-axis is the distance to the centre of the galaxy in kpc. For large r , the velocity becomes constant, which is called the flat rotation curve.

Zwicky also proposed a solution to this problem: dark matter [25]. With a certain dark matter distribution the flat rotation curves can be explained. For the Coma Cluster, from current observations a dark matter mass of 10 times the visible mass is needed to achieve the speeds of the galaxies in this cluster [11]. Dark matter distributions are thus fitted in a way such that these flat rotation curves follow, assuming certain general astrophysical properties the dark matter halos should obey. Apparent dark matter can however only be

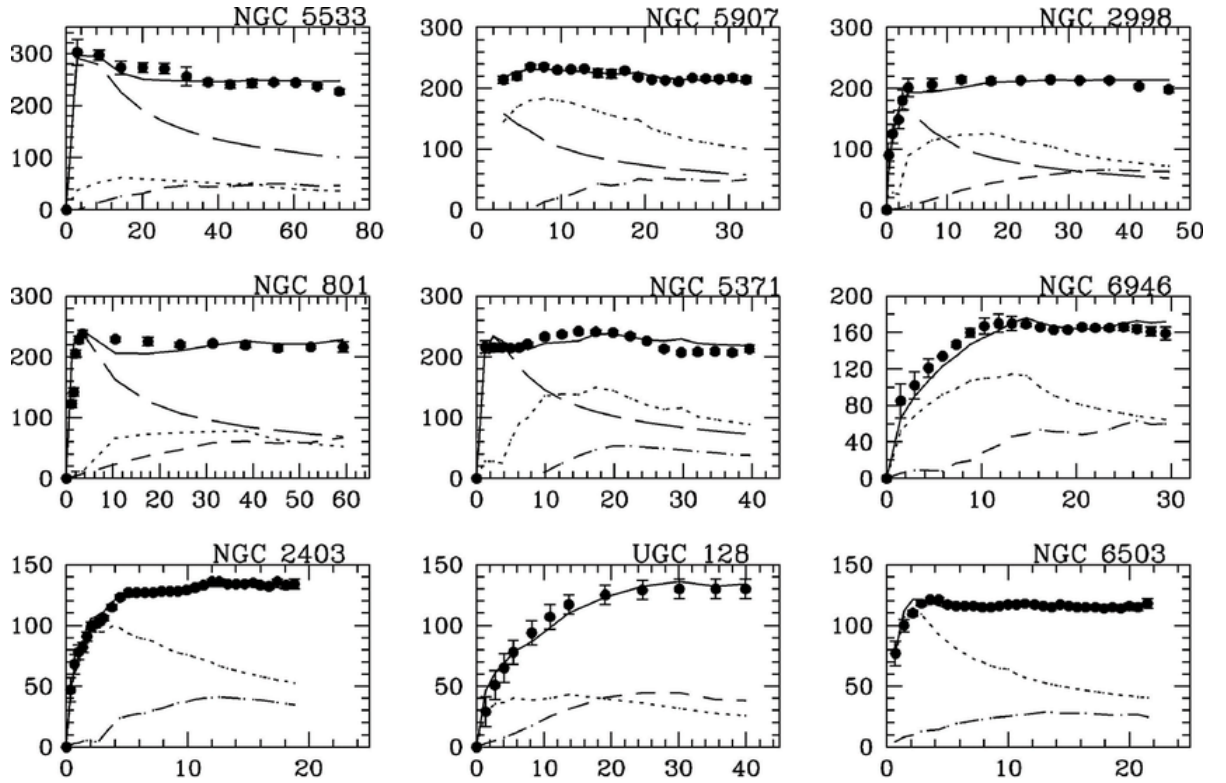


Figure 1.2: Rotation curves of galaxies. The filled circles are data observations, the solid line is the MOND rotation curve, the dotted and the dashed lines are Newtonian rotation curves due to visible and gaseous components. [18]

indirectly 'observed' by gravitational lensing [21]. For this thesis, we will not describe how dark matter distributions are obtained and how gravitational lensing works, but focus on an alternative solution.

In 1983, Milgrom proposed an alternative solution to the problem of the flat rotation curves. The flat rotation curves can be obtained by modifying Newtonian Dynamics: Modified Newtonian Dynamics (MOND) [13]. All galaxies approach a constant velocity for larger radii. Based on this, Milgrom introduced a new empirical constant: $a_0 = (1.2 \pm 0.2) \cdot 10^{-10} m/s^2$, which is a value for the acceleration which separates the gravitational behaviour for accelerations below and above this constant. In section 3 more information will be given on the accelerations and the gravitational potential in MOND. The modification should have a few important properties. First, by observing that the accelerations range from large to very small in galaxies and galaxy clusters, we need to have that for relatively large accelerations ($\gg a_0$), the modified theory should be in accordance with Newton. Furthermore, the modification should result in the flat rotation curve for the low acceleration regime ($\ll a_0$). One can obtain such a theory by modifying Newton's inertia law or gravity law. In this thesis, only the gravity law will be modified. Using MOND, dark matter is not necessary anymore for explaining the flat rotation curves. In figure 1.2 the empirical data of a few galaxies are compared to the rotation curve obtained by applying MOND to the visible and gaseous components. In section 3, MOND will be described mathematically and a possible explanation of the theory will also be given. This explanation also leads to MOND at accelerations much lower than a_0 and ND at accelerations much higher than a_0 and an interpolation function that combines these 2 regimes. There are also many other interpolation functions that have this characteristic which all lead to a different equation for MOND. In total 3 interpolation functions will be studied in this thesis.

Most observations made already have been used to deduce dark matter distributions assuming ND. It is thus useful to compare the results MOND predicts to the deduced dark matter distributions. Using the MOND potential, it is possible to construct the apparent dark matter. In this thesis we will compare the apparent dark matter extracted from MOND with the deduced dark matter distributions. The focus in this paper will be on a galaxy cluster: the Bullet Cluster. The Bullet Cluster is a special galaxy cluster, which was created by two colliding galaxy clusters. The Bullet Cluster is considered as strong evidence for dark matter [10]. In

section 4, the Bullet Cluster will be described in more detail and an overview will be given on the evidence for dark matter in this cluster. In section 5, we create a model of a Bullet-like cluster and it will be explained how we will generate mass distributions according to this model. Also it will be explained how a Bullet-like cluster will be simulated and how the potential will be calculated using ND and MOND for all interpolation functions. A comparison between the predicted potential using ND and the predicted potential using MOND will be made in section 6. These potentials are used to derive the apparent dark matter distribution, which is then compared to the deduced dark matter distribution of the Bullet Cluster. Also the apparent dark matter distributions from MOND will be analysed when increasing the mass of the galaxies and the number of the galaxies in the generated mass distribution. After that the results will be discussed and some interpretations of the results in section 7. Finally a few conclusions will be stated in section 8 and recommendations for further research.

2

Newtonian gravitational potential

In this section, the Newtonian gravitational potential will be derived for a single point mass and multiple point masses. Furthermore the Poisson equation will be derived for the Newtonian gravitational potential. Also it will be derived how the velocity of orbitals scales with the potential.

2.1. Potential of point masses

Given 2 point masses with mass m_1 and m_2 , Newton's gravitational law is given as follows:

$$\mathbf{F}_{12} = -\frac{Gm_1m_2}{r^2}\hat{\mathbf{r}}, \quad (2.1)$$

in which \mathbf{F}_{12} is the force acting on point mass m_2 due to m_1 in N , $\hat{\mathbf{r}}$ is the unit vector pointing from the position of m_2 to m_1 , G is the gravitational constant in $m^3 kg^{-1} s^{-2}$ and r is the distance between point masses m_1 and m_2 . Newton's second law is

$$\mathbf{F} = m\mathbf{a} \quad (2.2)$$

in which \mathbf{a} is the acceleration in m/s^2 . It follows that the gravitational acceleration of mass m_2 due to m_1 is

$$\mathbf{a} = -\frac{Gm_1}{r^2}\hat{\mathbf{r}}. \quad (2.3)$$

It can be shown that the gravitational acceleration is curl free, so $\nabla \times \mathbf{a} = 0$. From this fact, it follows that \mathbf{a} has a scalar potential that can be defined by:

$$\phi(\mathbf{x}) = -\int_{\mathcal{O}}^{\mathbf{x}} \mathbf{a} \cdot d\mathbf{l}, \quad (2.4)$$

in which the integral is any line integral from a reference point \mathcal{O} to point \mathbf{x} . For this definition it follows that

$$\mathbf{a} = -\nabla\phi \quad (2.5)$$

Now for a point mass m_1 , the potential at point \mathbf{x} is given by:

$$\phi(\mathbf{x}) = -\int_{\mathcal{O}}^{\mathbf{x}} -\frac{Gm_1}{r^2}\hat{\mathbf{r}} \cdot d\mathbf{l}. \quad (2.6)$$

Due to spherical symmetry, the potential can be written as a function of distance r from the point mass. By choosing the reference point \mathcal{O} at ∞ , the potential is given as follows:

$$\phi(r) = -\int_{\infty}^r -\frac{Gm_1}{r'^2} dr' = -\frac{Gm_1}{r}. \quad (2.7)$$

For multiple point masses, the potentials add up linearly. So the potential of N point masses m_i with $i \in \{1, 2, \dots, N\}$ placed at \mathbf{x}_i respectively, is as follows:

$$\phi(\mathbf{x}) = -\sum_{i=1}^N \frac{Gm_i}{\|\mathbf{x} - \mathbf{x}_i\|} \quad (2.8)$$

2.2. The Poisson equation

In this thesis, it will be useful to look at the potential using a differential equation, namely the Poisson equation. To derive the Poisson equation, we first state the divergence theorem:

Theorem 1 (Gauss) *Suppose V is a subset of \mathbb{R}^3 which is compact and has a piecewise smooth boundary S . If \mathbf{F} is a continuously differentiable vector field defined on a neighbourhood of V , then*

$$\iiint_V (\nabla \cdot \mathbf{F}) dV = \oiint_S (\mathbf{F} \cdot \hat{\mathbf{n}}) dS, \quad (2.9)$$

in which the left side is a volume integral over the volume V , the right side is a surface integral over the boundary S and $\hat{\mathbf{n}}$ is the outward pointing normal of the surface S .

Now we start with the gravitational acceleration due to a point mass M :

$$\mathbf{a} = -\frac{GM}{r^2} \hat{\mathbf{r}}, \quad (2.10)$$

in which again r is the distance to M and $\hat{\mathbf{r}}$ is radial outward pointing unit vector. Take a spherical volume V with surface S with the point mass in the center. Then we have that the outward pointing normal of the surface is just $\hat{\mathbf{r}}$. We can then calculate a surface integral:

$$\oiint_S \mathbf{a} \cdot \hat{\mathbf{r}} dA = \oiint_S -\frac{GM}{r^2} \hat{\mathbf{r}} \cdot \hat{\mathbf{r}} dA = -\frac{GM}{r^2} \oiint_S dA = -\frac{GM}{r^2} 4\pi r^2 = -4\pi GM. \quad (2.11)$$

Also it is true that:

$$\iiint_V \rho dV = M, \quad (2.12)$$

so we can write:

$$\oiint_S \mathbf{a} \cdot \hat{\mathbf{r}} dA = -4\pi GM = -4\pi G \iiint_V \rho dV = \iiint_V -4\pi G \rho dV. \quad (2.13)$$

But then by the divergence theorem, we have:

$$\nabla \cdot \mathbf{a} = -4\pi G \rho, \quad (2.14)$$

and using equation 2.5, we finally obtain the Poisson equation:

$$\nabla \cdot \nabla \phi = 4\pi G \rho. \quad (2.15)$$

We started with only a point mass, but because equation 2.15 is linear, the Poisson equation describes any arbitrary mass distribution.

2.3. Shell theorem

Point masses do not exist in nature. But in classical mechanics, the shell theorem provides a good use for the potential of a point mass. The shell theorem is as follows:

Theorem 2 *A spherical symmetric mass body affects external objects as though all of its mass were concentrated at a point in the center.*

This theorem was proved by Isaac Newton [14] and this allows us to simplify spherical symmetric mass distributions to point masses outside the spherical mass distribution. We will give another derivation to the shell theorem here. First we start with equation 2.11. We know by symmetry that the potential of a spherical symmetric mass distribution is also spherical symmetric. So we can write:

$$\mathbf{a} = a(r) \hat{\mathbf{r}} \quad (2.16)$$

in which $a(r)$ is a scalar function only dependent on the distant r to the center of the mass distribution. But then the surface integral can be rewritten:

$$\oiint_S \mathbf{a} \cdot \hat{\mathbf{r}} dA = \oiint_S a(r) \hat{\mathbf{r}} \cdot \hat{\mathbf{r}} dA = a(r) \oiint_S dA = a(r) 4\pi r^2 \quad (2.17)$$

and in equation 2.11, it follows that:

$$a(r) 4\pi r^2 = -4\pi GM \quad (2.18)$$

and this results in:

$$a(r) = \frac{GM}{r^2} \quad (2.19)$$

which is the same as equation 2.3.

2.4. Velocity of orbitals

In section 1, it was mentioned that the velocity of stars and galaxies is proportional to $\frac{1}{\sqrt{r}}$ for r large enough, in which r is the distance of the stars or galaxies to the center. This is the case when most mass is located in the center. If we assume the galaxy cluster to be spherically symmetric, then by the shell theorem, all mass can be replaced by a point mass in the center of the distribution for masses outside the mass density. This is the case for the stars or galaxies that orbit far from the center of the galaxy or galaxy cluster. In this thesis it will be derived for circular orbits. This assumption makes it a lot easier as the radius of the orbit will be constant. For a circular orbit, we have that the centripetal force is equal to the gravitational force [7]:

$$\frac{mv^2}{r} = \frac{GMm}{r^2} \quad (2.20)$$

in which m is the mass orbiting mass M , v is the velocity of mass m and r is the radius of the orbit. By the assumption that most mass is in the center, M is not dependent on r . This means that when r remains constant for orbits, so does v . By rewriting it, we obtain:

$$v = \sqrt{\frac{GM}{r}} \quad (2.21)$$

We see that $v \propto \frac{1}{\sqrt{r}}$ under the assumptions stated above. This relation is for example also correct for the planets in the solar system, which also follows from Kepler's second law [7].

3

MOND

In this section, Modified Newtonian Dynamics or MOND will be explained in more detail. First MOND will be described mathematically and its requirements will be stated. Then a possible explanation will be given for MOND and finally some possible interpolation functions will be given.

3.1. The MOND equations

As mentioned in the introduction, the theory is aimed to explain a flat rotation curve for accelerations much lower than Milgrom's constant a_0 , which is $1.2 \cdot 10^{-10} m/s^2$ and result in Newton's gravity law for accelerations much higher than a_0 . To achieve this, the gravity law is modified. The Newtonian gravity law is as follows:

$$a = \frac{GM}{r^2}. \quad (3.1)$$

In MOND, for low accelerations ($a \ll a_0$), the equation becomes:

$$\frac{a^2}{a_0} = \frac{GM}{r^2}. \quad (3.2)$$

These two equations can be combined into one:

$$\mu\left(\frac{a}{a_0}\right) a = \frac{GM}{r^2}, \quad (3.3)$$

in which μ is a function of $\frac{a}{a_0}$, which will be called an interpolation function. By comparing equations 3.1 and 3.2 to equation 3.3, the interpolation function should satisfy the following conditions:

$$\mu(x) = \begin{cases} x, & x \ll 1 \\ 1, & x \gg 1. \end{cases} \quad (3.4)$$

To see how changing the gravity law in this manner results in the flat rotation curves, we start by writing out the deep MOND equation again valid for $a \ll a_0$:

$$F_N = m \frac{a^2}{a_0}, \quad (3.5)$$

in which F_N is the classical gravitational force. For circular orbits the acceleration in classical mechanics can be written as follows:

$$a = \frac{v^2}{r}. \quad (3.6)$$

Now combining the equations results in:

$$\frac{GMm}{r^2} = \frac{m\left(\frac{v^2}{r}\right)^2}{a_0}, \quad (3.7)$$

and finally:

$$v^4 = GMa_0. \quad (3.8)$$

As can be seen, the velocity is independent of r .

In section 2, the Poisson equation was derived for the Newtonian gravitational potential. Also remember that $\mathbf{a} = -\nabla\phi$, in which \mathbf{a} is the acceleration and ϕ is the Newtonian gravitational potential. For MOND, similarly we will assume: $\mathbf{a} = -\nabla\phi_M$, in which ϕ_M is the MOND potential. By the requirements stated above, for accelerations much larger than a_0 , we should still have the poisson equation for the MOND potential:

$$\nabla \cdot \nabla\phi_M = 4\pi G\rho. \quad (a \gg a_0). \quad (3.9)$$

For accelerations much lower than a_0 , Milgrom proposed a different differential equation [13]:

$$\nabla \cdot \left(\frac{|\nabla\phi_M|}{a_0} \nabla\phi_M \right) = 4\pi G\rho. \quad (a \ll a_0). \quad (3.10)$$

So by equation 3.4, MOND has the following differential equation:

$$\nabla \cdot \left(\mu \left(\frac{|\nabla\phi_M|}{a_0} \right) \nabla\phi_M \right) = 4\pi G\rho. \quad (3.11)$$

3.2. Verlinde interpolation

In 2010, Eric Verlinde published a paper in which he derived the Newtonian gravity law from entropic forces [23]. In this paper, he modified Bekenstein's thought experiment [2] at the surface of a black hole to an arbitrary holographic surface. Using this method, Newtonian gravity can be derived. Later in 2017, he published another paper in which he proposed a solution to the missing mass problem, emergent gravity, starting from a microscopic theory [24]. For point masses, his theory complies with the MOND equations with a certain interpolation function. In this thesis, the interpolation function derived from his findings will be referred to as the Verlinde interpolation function. Verlinde's derived connection between Newtonian gravitational acceleration and the actual acceleration for point masses is given by the following formula:

$$\mathbf{a} = \mathbf{a}_N + \sqrt{\frac{a_0}{a_N}} \mathbf{a}_N, \quad (3.12)$$

in which \mathbf{a} is the actual acceleration in m/s^2 , \mathbf{a}_N is the acceleration predicted by Newtonian gravity in m/s^2 , $a_N = |\mathbf{a}_N|$ and a_0 is Milgrom's constant in m/s^2 . It is useful to write the acceleration derived from Newtonian gravity as a function of the actual acceleration, so that it can be substituted in the Poisson equation. This function divided by \mathbf{a} is the scalar Verlinde interpolation function μ_v . As the actual acceleration is in the same direction as the Newtonian gravitational acceleration, we can work with the lengths of the accelerations, so $\mathbf{a} = a\hat{\mathbf{a}}$ and $\mathbf{a}_N = a_N\hat{\mathbf{a}}_N = a_N\hat{\mathbf{a}}$. To obtain this function, first we substitute $y = \sqrt{a_N}$. So we get the following equation:

$$a = y^2 + \sqrt{a_0}y. \quad (3.13)$$

This is a quadratic formula and can be solved for y , which results in:

$$\sqrt{a_N} = y = -\frac{1}{2}a_0 \pm \sqrt{a + \frac{1}{4}a_0}. \quad (3.14)$$

Now squaring the left side and the right side gives:

$$a_N = \frac{1}{2}a_0 + a \pm \sqrt{a_0} \sqrt{a + \frac{1}{4}a_0}. \quad (3.15)$$

Now because $a_N = \mu(a)a$, we have:

$$\mu_v(a) = \frac{1}{2a}a_0 + 1 \pm \frac{\sqrt{a_0} \sqrt{a + \frac{1}{4}a_0}}{a}. \quad (3.16)$$

Rewriting this, we get:

$$\mu_v(a) = \frac{\pm 4 \frac{\sqrt{a + \frac{1}{4}a_0}}{\sqrt{a_0}} + 4 \frac{a}{a_0} + 2}{4 \frac{a}{a_0}}. \quad (3.17)$$

Now by doing another substitution $x = \frac{a}{a_0}$, we finally obtain:

$$\mu_v(x) = \frac{\pm 4\sqrt{x+1/4} + 4x + 2}{4x} = \frac{(\sqrt{1+4x} \pm 1)^2}{4x}. \quad (3.18)$$

Now μ_v should satisfy condition 3.4. For the plus sign, it does not satisfy these conditions so finally:

$$\mu_v(x) = \frac{(\sqrt{1+4x} - 1)^2}{4x}. \quad (3.19)$$

Now Verlinde's theory can be written as in equation 3.3 with $\mu(x) = \mu_v(x)$.

3.3. Other interpolation functions

Besides Verlinde's interpolation function, many others can be constructed which satisfy condition 3.4. All of the following interpolation functions are functions of $x = \frac{a}{a_0}$. The standard interpolation function is as follows:

$$\mu_s(x) = \frac{x}{\sqrt{1+x^2}}, \quad (3.20)$$

which is also used by Milgrom. Another interpolation function is a parametrized function [1]:

$$\mu_{\text{angus}}(x) = \frac{2x}{1 + (2 - \alpha)x + \sqrt{(1 - \alpha x)^2 + 4x}}, \quad (3.21)$$

with $0 \leq \alpha \leq 1$. It can be checked that the Verlinde interpolation function is the same as choosing $\alpha = 0$. In this thesis we will also look at the interpolation function for $\alpha = 1$. This results in:

$$\mu_{\text{angus}}(x) = \frac{x}{1+x}. \quad (3.22)$$

This interpolation function will be referred to as the Angus interpolation function in this thesis. All the interpolation functions are plotted in figure 3.1 as a function of x . Also the actual acceleration, which can be obtained by inverting the interpolation functions, are plotted against the Newtonian gravitational acceleration in figure 3.2. In figure 3.3, a few similar interpolation functions are plotted with observed data points [4].

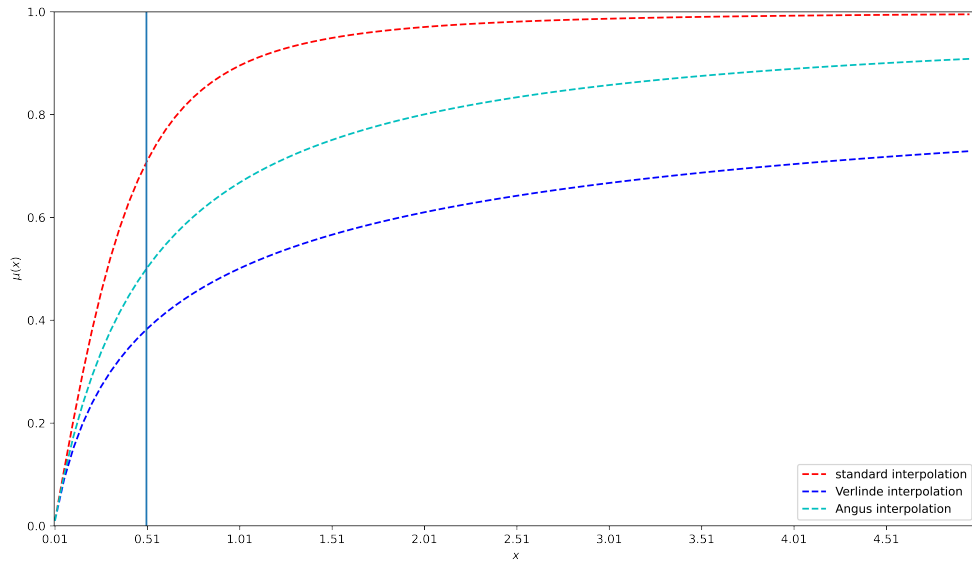


Figure 3.1: Plot of the interpolation functions mentioned in this chapter. As can be seen, the interpolation functions satisfy $\mu(x) \rightarrow 1$ for $x \rightarrow \infty$. For the Angus interpolation function, α is chosen to be 1.

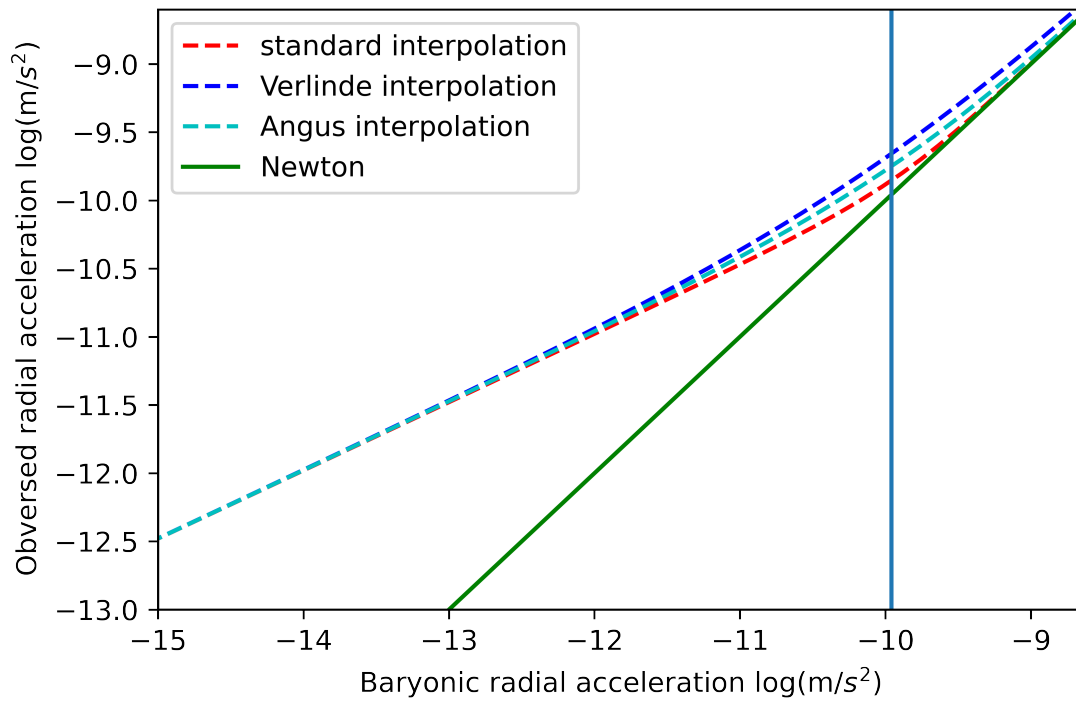


Figure 3.2: Plot of the actual acceleration for the different mentioned interpolation functions against the Newtonian acceleration due to observed mass. For the Angus interpolation function, α is chosen to be 1.

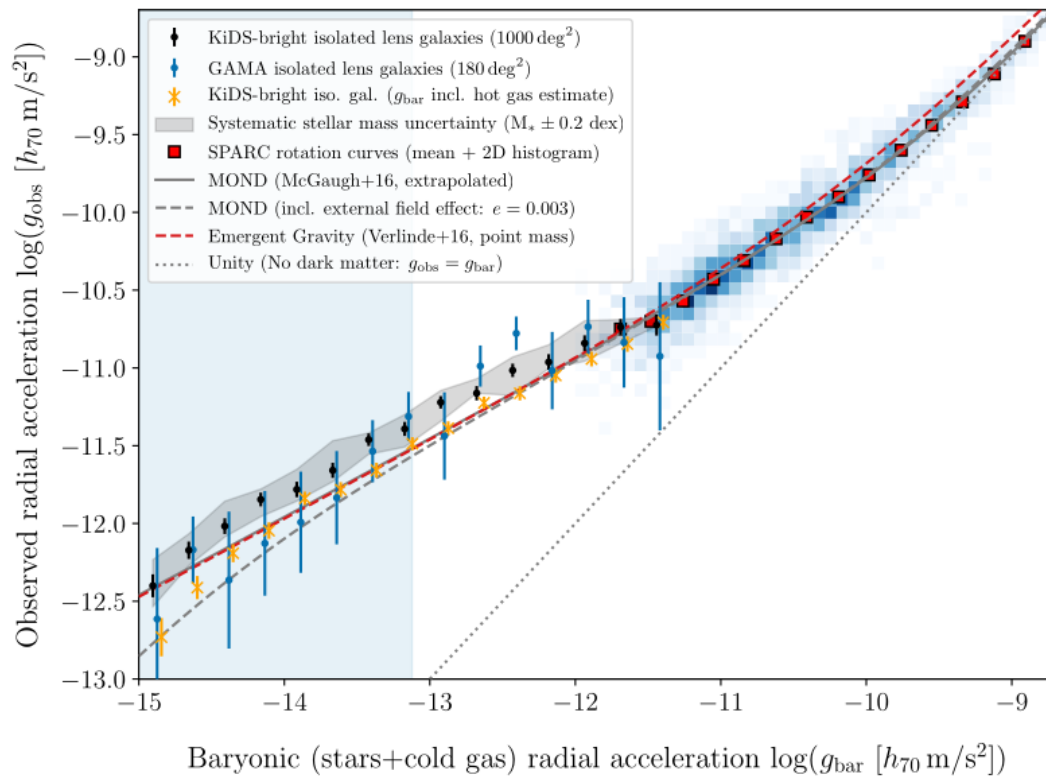


Figure 3.3: Plot of the actual acceleration against the Newtonian acceleration due to observed mass. Also observed data points are added.
[4]

4

Bullet Cluster

The Bullet Cluster(1E 0657-56) is a galaxy cluster which consists of two colliding sub galaxy clusters [22]. One sub-cluster, the "bullet" has collided with the main cluster, which resulted in a distinct offset between the baryonic mass components [9]. This offset led to a special possibility to measure the mass distribution using gravitational lensing studies, which seemed to prove the theory of dark matter and especially seemed to falsify popular MOND theories. This is because the majority of the mass is spatially coincident with the galaxies and not the intra-cluster gas [10] [3], while the mass of the intracluster gas is around ten times heavier than the total mass of the galaxies [6]. However, in 2006 a paper was released in which it would be left open if MOND or it's relativistic version TeVeS could explain the Bullet Cluster in non spherically symmetric cases [1]. Also Milgrom himself wrote a short rebuttal online on the evidence of dark matter due to the Bullet Cluster [12], in which he states that it has been known for a long time already that MOND does not fully explain the mass discrepancy in galaxy clusters. He did not propose a solution but stated that it is probable that not all baryonic matter has been observed yet.

The Bullet Cluster can be modelled with separate baryonic and dark matter components. In this thesis we will reconstruct the dark matter model in the paper of Paraficz et al [15]. In this paper, the dark matter components are three dark matter halos, two for the main cluster and one for the sub-cluster. The baryonic components consist of two things: the intra-cluster gas and the two galaxy subclusters. In this thesis we will also replicate the gas model of Paraficz et al.

The intracluster gas mass distribution can be measured with from their X-ray emission and generally are 10% to 15% of the total mass of the galaxy cluster [6]. In this thesis, the gas mass will be modelled with a spherical mass density. The mass density as described in the paper of Paraficz et al is a projected mass surface density [15]. An approximation for the 3D gas density can be made, which is the following:

$$\rho_{\text{gas}}(r) = 2\rho_{\text{gas},0} \frac{1}{\left(1 + \frac{r^2}{r_c^2}\right)}. \quad (4.1)$$

The parameters found in the paper are: $\theta_c = 112.5''$, for which $1'' = 4.413 \text{ kpc}$, $n_{e0} = 7.2 \cdot 10^{-3}$ is the number of electrons per cm^3 . This is the same as $r_c = 112.5 \cdot 4.413 = 496.6 \text{ kpc}$ and $\rho_{\text{gas},0} = 1.205 \cdot 10^{-23} \text{ kg/m}^3$, assuming that the number of electrons is equal to the number of protons.

The dark matter clumps are modelled as Pseudo Isothermal Elliptical mass distributions or PIsEmd in the paper of Paraficz et al. In this thesis we are interested in the projected mass density profile, which is the mass density in kg/m^3 projected on an axis. This is done by integrating the mass density over a certain coordinate. Images of galaxy clusters are two dimensional, the distance between the observer and the observed object can not be derived from an image. The mass density is thus integrated in this direction, resulting in the projected mass density profile. The projected mass density profile in kg/m^2 for a PIsEmd is given by the following formula [8]:

$$\Sigma(R) = \frac{\sigma_0^2 r_{\text{cut}}}{2\pi G} \left(\frac{1}{\sqrt{r_{\text{core}}^2 + R^2}} - \frac{1}{\sqrt{r_{\text{cut}}^2 + R^2}} \right) \frac{1}{r_{\text{cut}} - r_{\text{core}}}, \quad (4.2)$$

in which σ_0 is the velocity dispersion in m/s , R is position on the projected plane, r_{core} is a radius in m for which the 3 dimensional mass density $\approx r^{-2}$ for distances $\gg r_{\text{core}}$, r_{cut} is the radius in m at which 3 dimen-

	$\Delta\alpha$ (")	$\Delta\delta$ (")	r_{core} (kpc)	r_{cut} (")	σ_0 (km s ⁻¹)
DM1	8.3	-2.5	117.4	1000	884.2
DM2	24.1	28.3	127.3	1000	840.2
DM3	185.9	50.1	47.3	1000	795.7

Table 4.1: Table with the optimized parameters for the the dark matter clumps (DM) found in the paper of Paraficz et al [15]. $\Delta\alpha$ corresponds to the x coordinate, $\Delta\delta$ corresponds to the y coordinate. An image is only 2 dimensional so the coordinates are only in two dimensions. Furthermore " corresponds to 4.413 kpc.

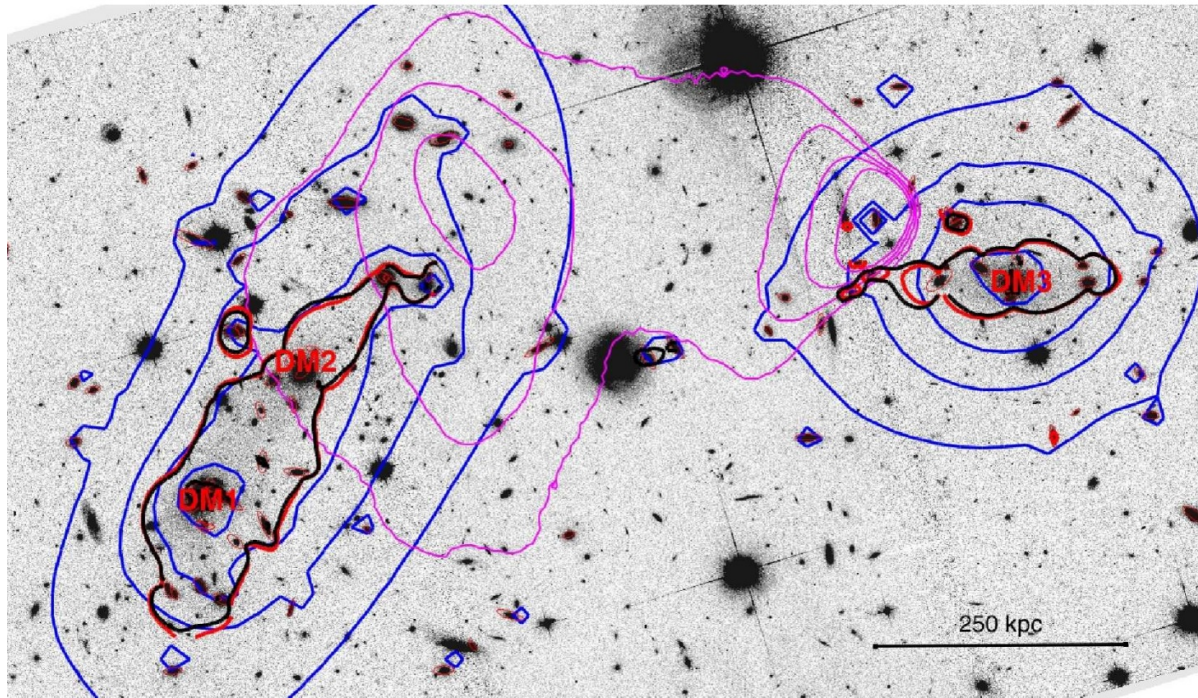


Figure 4.1: F606W-band image of the Bullet cluster. The magenta contours represent the X-ray brightness map, the blue contours show the projected mass density [15]. The contours with other colors are not relevant for this thesis.

sional mass density $\simeq r^{-4}$ for distances $\gg r_{\text{cut}}$. In the paper of Paraficz et al, the projected mass densities are also modelled as ellipsoids, but in this thesis we will model the projected distributions as circular. For the purposes in this thesis, only the optimized parameters of the dark matter clumps are used, which are in stated in table 4.1.

5

Generation of the model and numerical solutions

In this chapter, the model used will be explained. First the generation of a Bullet-like cluster will be described. Then it will be explained how the Poisson equation can be solved analytically and then numerically using the Fourier transform or the Fast Fourier Transform. Also the Helmholtz decomposition with Fourier transforms will be introduced. Finally a method will be described to solve the MOND differential equation numerically with an iterative method.

5.1. Modelling a Bullet cluster-like cluster

In this section, the generation of the mass distribution in this thesis based on the Bullet Cluster will be described.

5.1.1. Discretization of volume of space

The Bullet cluster consists of two originally smaller clusters. The sub-clusters are placed to the left and to the right of the intra-cluster gas. We take the diameter of the cluster to be $L = 2$ Mpc, as can be seen in figure 5.1. To be able to simulate a Bullet cluster-like cluster, we need to be able to give an input to the computer, which means an array of discrete values. The input mass density will be a 3D array, with size $N \times N \times N$. N is chosen to be 512 in this thesis. This array needs to describe the entire mass distribution. To avoid edge effects in the computation method (which will be explained later), we will simulate $2L \times 2L \times 2L$. This means that each element in the starting array will represent the mass in a cube of $2L/N \times 2L/N \times 2L/N$, which is around 480 kpc^3 .

5.1.2. Generation of the mass distribution

First we need a way to randomize the mass distribution in a way such that it resembles the Bullet Cluster described in section 4. As already said, the baryonic matter consists of two components, the galaxies and the intracluster gas. The intracluster gas is modelled as a sphere with density described by equation 4.1. Also the center of the intracluster gas is placed at the origin. In total 40 galaxies are placed with the a tenth of the virial mass of the Milky Way. The virial mass of the Milky Way is $1.26 \cdot 10^{12} M_{\odot}$. Thus in this paper the mass of the Milky Way is chosen to be $M_{\text{Milky-Way}} = 1.26 \cdot 10^{11} M_{\odot}$. This is done because we want to only use baryonic mass and the estimated baryonic mass of galaxies is 0.1 times the virial mass. The galaxies are generated spherically symmetric around 2 positions \mathbf{x}_1 and \mathbf{x}_2 , which are estimated from figure 4.1. The galaxies are modelled as spheres with the radius of the milky way, which is $R_{\text{Milky Way}} = 52.85$ light year [16]. We took the estimated center of the intracluster gas as the origin and placed \mathbf{x}_1 and \mathbf{x}_2 in the xy-plane at the positions $\mathbf{x}_1 = (-370, -130, 0)$ kpc and $\mathbf{x}_2 = (370, 40, 0)$ kpc.

In the main cluster we will simulate 25 galaxies and in the subcluster 15 galaxies. In order to generate the galaxies spherically symmetric, we will work in spherical coordinates ϕ , θ and r . To randomise ϕ and θ , we will use the distribution as in the thesis by Odessa Schokker [19]:

$$\theta = 2\pi u \tag{5.1}$$

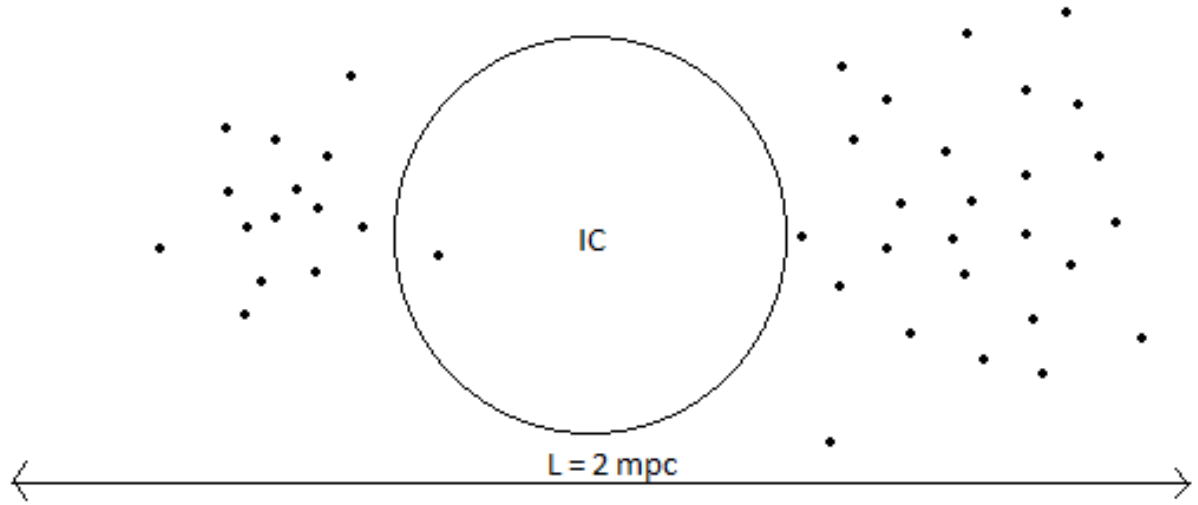


Figure 5.1: The model used in this thesis for the Bullet Cluster projected onto the xy -plane. The intra-cluster gas is indicated by the circle with IC. The dots are the galaxies. The galaxies are placed randomly according to spherically symmetric distributions around 2 different points (see text).

$$\phi = \arccos(2\nu - 1) \quad (5.2)$$

in which u and ν are uniform random variables on the interval $[0, 1]$.

To randomise r , we begin with the assumption that galaxies formed from a gas cloud, with the same mass distribution as the intracluster gas. The cumulative distribution function $F(r)$ for the radial coordinate r is calculated by the mass in a radius of r divided by the total mass M :

$$F(r) = \int_0^r \pi r'^2 \frac{1}{M} \frac{2\rho_0}{1 + \frac{r'^2}{r_c^2}} dr' = \frac{8\pi\rho_0}{M} r_c^2 \left(r - r_c \arctan\left(\frac{r}{r_c}\right) \right). \quad (5.3)$$

Now the mass distribution of a gas does not extend to infinity, so we choose a radius at which we set the density to zero, r_{cutoff} . This leads to a way to also calculate M :

$$M = \int_0^{r_{\text{cutoff}}} \pi r'^2 \frac{2\rho_0}{1 + \frac{r'^2}{r_c^2}} dr' = 8\pi\rho_0 r_c^2 \left(r_{\text{cutoff}} - r_c \arctan\left(\frac{r_{\text{cutoff}}}{r_c}\right) \right). \quad (5.4)$$

Combining this with the equation 5.3 leads to:

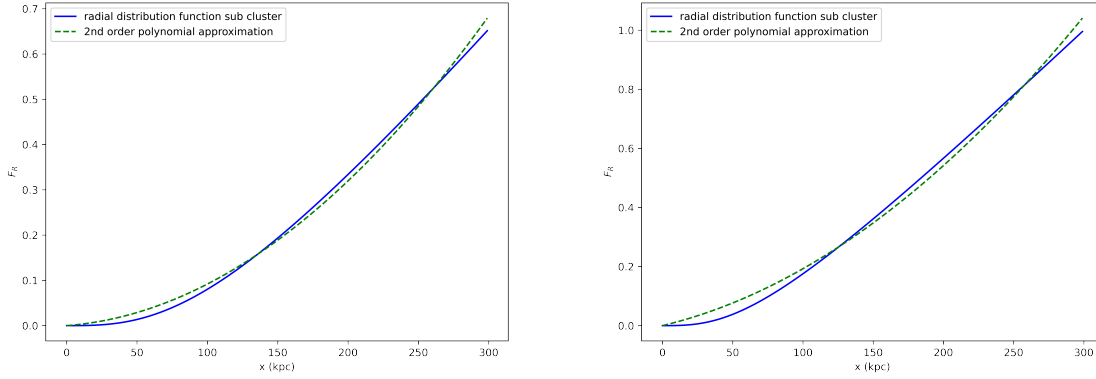
$$F(r) = \frac{r - r_c \arctan\left(\frac{r}{r_c}\right)}{r_{\text{cutoff}} - r_c \arctan\left(\frac{r_{\text{cutoff}}}{r_c}\right)}. \quad (5.5)$$

This is a cumulative distribution function. We want to generate sample values of this distribution function in a way that the samples have distribution function $F(r)$. Let W denote a random variable uniform on $[0, 1]$. Then the random variable $Y = F^{-1}(W)$ is the random variable that generates samples corresponding to the distribution function $F(r)$. This can be seen as follows:

$$P(Y < r) = P(F(Y)) < F(r) = P(W < F(r)) = F(r). \quad (5.6)$$

So we need to find an inverse function to distribution function $F(r)$. It is however not possible to find an analytical formula for the inverse of this function. To get an approximation of the inverse function, we fit a 2nd order polynomial $y = ax^2 + bx$ on the function using python. No offset is added, because we want $y = 0$ for $x = 0$. Then by inverting this polynomial and only taking the positive x values we obtain the following inverse function:

$$x = \sqrt{\frac{b^2}{4a^2} + \frac{y}{a}} - \frac{b}{2a}. \quad (5.7)$$



(a) Main cluster.

(b) Sub cluster.

Figure 5.2: The radial mass distribution functions for the main and sub cluster.

Now let W be a uniform random variable on the interval $[0,1]$ and w be samples from this random variable. Then:

$$r = F^{-1}(w) \approx \sqrt{\frac{b^2}{4a^2} + \frac{w}{a} - \frac{b}{2a}} \quad (5.8)$$

will result in the samples that correspond to the distribution function $F(r)$.

In this thesis r_{cutoff} is chosen at 400 kpc for the main cluster and 300 kpc for the sub cluster and r_c is chosen to be 100 kpc for the main cluster and 60 kpc for the sub cluster, which are estimated from figure 4.1. This results in $a_1 = 5.03 \cdot 10^{-6}$, $b_1 = 6.07 \cdot 10^{-4}$ corresponding to the inverse function for the radial distribution function of main cluster and $a_2 = 7.81 \cdot 10^{-6}$, $b_2 = 1.14 \cdot 10^{-3}$ for sub cluster. In figure 5.2 the approximated polynomials and the distribution functions are plotted.

5.2. Solving ND Numerically

The Newtonian gravitational potential can be obtained from the mass density by solving the Poisson equation, which we restate here:

$$\nabla \cdot \nabla \phi = 4\pi G \rho \quad (2.15 \text{ revisited})$$

This is a differential equation, which can be solved analytically for many different mass distributions ρ . In this thesis we will solve this differential equation using Fourier transforms. This method can then also be applied to solving the MOND equations, which have no analytic solutions in most cases. Also, in our model, the mass distribution is discretized, so to calculate the Fourier transform of this distribution, it is useful to introduce the Fast Fourier Transform (FFT). In the following sections the position vector will be denoted by \mathbf{r} or (x, y, z) and the wave vector in the Fourier domain will be denoted by \mathbf{k} or (k_x, k_y, k_z) .

5.2.1. Fourier transform

The Fourier transform pair of a function f mapping from \mathbb{R}^3 to \mathbb{R} is defined as follows:

$$\mathcal{F}\{f\}(\mathbf{k}) = (2\pi)^{-3/2} \iiint_{\mathbb{R}^3} f(\mathbf{r}) e^{-i\mathbf{k}\cdot\mathbf{r}} d\mathbf{r} \quad (5.9)$$

$$f(\mathbf{r}) = (2\pi)^{-3/2} \iiint_{\mathbb{R}^3} \mathcal{F}\{f\}(\mathbf{k}) e^{i\mathbf{k}\cdot\mathbf{r}} d\mathbf{k} \quad (5.10)$$

The Fourier transform pair of a function \mathbf{f} mapping from \mathbb{R}^3 to \mathbb{R}^3 is defined as follows:

$$\mathcal{F}\{\mathbf{f}\}(\mathbf{k}) = (2\pi)^{-3/2} \iiint_{\mathbb{R}^3} \mathbf{f}(\mathbf{r}) e^{-i\mathbf{k}\cdot\mathbf{r}} d\mathbf{r} \quad (5.11)$$

$$\mathbf{f}(\mathbf{r}) = (2\pi)^{-3/2} \iiint_{\mathbb{R}^3} \mathcal{F}\{\mathbf{f}\}(\mathbf{k}) e^{i\mathbf{k}\cdot\mathbf{r}} d\mathbf{k} \quad (5.12)$$

These definitions will be useful in deriving the following useful identity:

$$\mathcal{F}\{\nabla f\} = i\mathbf{k}\mathcal{F}\{f\}, \quad (5.13)$$

for scalar function $f(\mathbf{r})$ with $f(\mathbf{r}) \rightarrow 0$ for $|\mathbf{r}| \rightarrow \infty$. This is the differentiation identity of the Fourier transform.

By definition of the Fourier transform, the Fourier transform of the gradient of a function is given by:

$$\mathcal{F}\{\nabla f\}(\mathbf{k}) = (2\pi)^{-3/2} \iiint_{\mathbb{R}^3} \nabla f(\mathbf{r}) e^{-i\mathbf{k}\cdot\mathbf{r}} d\mathbf{r}. \quad (5.14)$$

This can be written as

$$\mathcal{F}\{\nabla f\}(\mathbf{k}) = (2\pi)^{-3/2} \left(\iiint_{\mathbb{R}^3} \frac{\partial}{\partial x} f(\mathbf{r}) e^{-i\mathbf{k}\cdot\mathbf{r}} d\mathbf{r}, \iiint_{\mathbb{R}^3} \frac{\partial}{\partial y} f(\mathbf{r}) e^{-i\mathbf{k}\cdot\mathbf{r}} d\mathbf{r}, \iiint_{\mathbb{R}^3} \frac{\partial}{\partial z} f(\mathbf{r}) e^{-i\mathbf{k}\cdot\mathbf{r}} d\mathbf{r} \right). \quad (5.15)$$

Then using partial integration and $f(\mathbf{r}) \rightarrow 0$ for $|\mathbf{r}| \rightarrow \infty$, the following is obtained:

$$\mathcal{F}\{\nabla f\}(\mathbf{k}) = (2\pi)^{-3/2} \left(\iiint_{\mathbb{R}^3} ik_x f(\mathbf{r}) e^{-i\mathbf{k}\cdot\mathbf{r}} d\mathbf{r}, \iiint_{\mathbb{R}^3} ik_y f(\mathbf{r}) e^{-i\mathbf{k}\cdot\mathbf{r}} d\mathbf{r}, \iiint_{\mathbb{R}^3} ik_z f(\mathbf{r}) e^{-i\mathbf{k}\cdot\mathbf{r}} d\mathbf{r} \right), \quad (5.16)$$

and this then combines into equation 5.13. The Fourier transform of a function \mathbf{f} mapping from \mathbb{R}^3 to \mathbb{R}^3 also has such an identity:

$$\mathcal{F}\{\nabla \cdot \mathbf{f}\} = i\mathbf{k} \cdot \mathcal{F}\{\mathbf{f}\} \quad (5.17)$$

, which has a similar derivation.

In section 2, the scalar Newtonian gravitational potential was defined. To solve the Poisson equation, we set our reference point at ∞ again. That way, $\phi(\mathbf{r}) \rightarrow 0$ for $|\mathbf{r}| \rightarrow \infty$. Now we are able to use the Fourier transform on the left and use the differentiation identity, which leads to:

$$-\mathbf{k} \cdot \mathbf{k} \mathcal{F}\{\phi\} = 4\pi G \mathcal{F}\{\rho\}. \quad (5.18)$$

Rewriting this, and taking the inverse Fourier transform, we obtain a solution:

$$\phi = -4\pi G \mathcal{F}^{-1} \left\{ \frac{\mathcal{F}\{\rho\}}{\mathbf{k} \cdot \mathbf{k}} \right\}, \quad (5.19)$$

if $\mathbf{k} \neq \mathbf{0}$. By also choosing $\phi(\mathbf{0}) = 0$ we can obtain an unique solution.

5.2.2. Fast Fourier Transform

In our model, the mass density $\rho(\mathbf{r})$ are discrete values at discrete positions, so a numerical approximation to the actual mass density. A numerical approximation to calculate the Fourier transform is the Fast Fourier Transform. The Fast Fourier Transform has as input discrete values, and as output again discrete values, so it fits well in our model. The Fast Fourier Transform pair is defined as follows:

$$X_{\mathbf{k}} = \frac{1}{N^3} \sum_{\mathbf{n}=0}^{N-1} x_{\mathbf{n}} e^{-2\pi i \mathbf{k}\cdot\mathbf{n}/N} \quad (5.20)$$

$$x_{\mathbf{n}} = \sum_{\mathbf{k}=0}^{N-1} X_{\mathbf{k}} e^{2\pi i \mathbf{k}\cdot\mathbf{n}/N} \quad (5.21)$$

The FFT has input and also output which are periodic with period N . This means that it calculates the FFT as if there were an infinite lattice of N by N by N cubes with the same initial conditions. Therefore the border of our model is significantly influenced by the initial conditions at the other end of our model. To combat this problem, in our model we only look at the result in the center of our plot, so only the elements $x_{\mathbf{n}}$ from $1/4N$ to $3/4N$ in our cube, in all three directions.

5.2.3. Analytic calculation vs numerical approximation of 2 point masses

In section 2, the potential was derived for multiple point masses in equation 2.8. We can compare this analytic result with the numerical approximation obtained with the Fourier method described above for a system with 2 point masses with $m = 10^{14} M_{\odot}$, which are placed at $\mathbf{r}_1 = (-312.5, 0, 0)$ kpc and $\mathbf{r}_2 = (312.5, 0, 0)$ kpc. The approximation is very accurate as can be seen in figure 5.3.

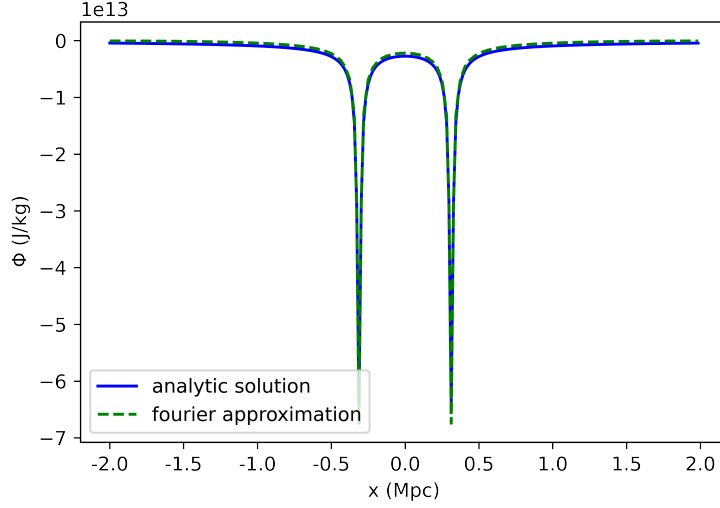


Figure 5.3: The analytic and Fourier approximation of the Newtonian gravitational potential as a function of r_x of 2 point masses for r_y and r_z equal to 0. The point masses both have mass $10^{14} M_\odot$.

5.3. Helmholtz decomposition with Fourier transform

It is possible to decompose a three-vector field into a longitudinal and transverse component [20]. So a vector field \mathbf{F} mapping from \mathbb{R}^3 to \mathbb{R}^3 , can be written as:

$$\mathbf{F} = \mathbf{F}_\parallel + \mathbf{F}_\perp, \quad (5.22)$$

with $\nabla \times \mathbf{F}_\parallel = 0$ and $\nabla \cdot \mathbf{F}_\perp = 0$. It is useful to write this using Fourier transforms. For that we introduce the following notation: $\mathcal{F}\{f\}(\mathbf{k}) = \tilde{f}(\mathbf{k})$. $\tilde{\mathbf{F}}(\mathbf{k}) = \tilde{\mathbf{F}}_\parallel(\mathbf{k}) + \tilde{\mathbf{F}}_\perp(\mathbf{k})$ due to linearity of the Fourier transform. By the differentiation identity, we also know $i\mathbf{k} \cdot \tilde{\mathbf{F}}_\perp = 0$. The Fourier also has a similar characteristic for the curl [], which leads $i\mathbf{k} \times \tilde{\mathbf{F}}_\parallel = 0$. To find $\tilde{\mathbf{F}}_\parallel$ and $\tilde{\mathbf{F}}_\perp$, we can use projections in the Fourier domain. This leads to the following equations:

$$\tilde{\mathbf{F}}_\parallel = \frac{\mathbf{k} \cdot \tilde{\mathbf{F}}}{\mathbf{k} \cdot \mathbf{k}} \mathbf{k}, \quad (5.23)$$

$$\tilde{\mathbf{F}}_\perp = \tilde{\mathbf{F}} - \frac{\mathbf{k} \cdot \tilde{\mathbf{F}}}{\mathbf{k} \cdot \mathbf{k}} \mathbf{k}. \quad (5.24)$$

5.4. Solving MOND Numerically

For MOND, we need to solve another differential equation, which we state here again:

$$\nabla \cdot \left(\mu \left(\frac{|\nabla \phi_M|}{a_0} \right) \nabla \phi_M \right) = 4\pi G \rho, \quad (3.11 \text{ revisited})$$

in which μ is an interpolation function and ϕ_M is the MOND potential. It is not possible to solve this differential equation analytically, however we can solve it iteratively using Fourier transforms. Now let's introduce a few useful substitutions. First $\mathbf{F} = -\mu \left(\frac{|\nabla \phi_M|}{a_0} \right) \nabla \phi_M$. Now equation 3.11 can be written as:

$$-\nabla \cdot \mathbf{F} = 4\pi G \rho. \quad (5.25)$$

We already know a solution to this problem, namely the Newtonian acceleration. But remember that a requirement for the Newtonian acceleration was $\nabla \times \mathbf{a}_N = 0$. In MOND however, this does not have to be the case for \mathbf{F} . Using the Helmholtz decomposition, we can write $\mathbf{F} = \mathbf{F}_\parallel + \mathbf{F}_\perp$. By equation 5.25, we have:

$$-\nabla \cdot \mathbf{F} = -\nabla \cdot (\mathbf{F}_\perp + \mathbf{F}_\parallel) = -\nabla \cdot \mathbf{F}_\perp - \nabla \cdot \mathbf{F}_\parallel = -\nabla \cdot \mathbf{F}_\parallel = 4\pi G \rho, \quad (5.26)$$

as we have $\nabla \cdot \mathbf{F}_\perp = 0$. So we know $\mathbf{F}_\parallel = \mathbf{a}_N$. \mathbf{F}_\perp remains unknown and will be called \mathbf{B} for now.

5.4.1. Inverse interpolation function

Looking at the MOND differential equation, it seems useful to also introduce the following vector: $\mathbf{f} = -\nabla\phi_M$. First note that $\nabla \times \mathbf{f} = 0$. Now by the definitions of \mathbf{f} and \mathbf{F} , they have the following relation:

$$\mathbf{F} = \mu\left(\frac{|\mathbf{f}|}{a_0}\right)\mathbf{f}. \quad (5.27)$$

So it is also possible to calculate \mathbf{f} if \mathbf{F} is known, which will be useful for the iterative method. First notice that \mathbf{F} and \mathbf{f} point in the same direction, they only differ by a scalar factor $\mu\left(\frac{|\mathbf{f}|}{a_0}\right)$. Let $f = |\mathbf{f}|$ and $F = |\mathbf{F}|$. The process for finding the inverse relation between F and f is the same for each interpolation function but the formula is different. In this thesis we will only show the derivation for the standard interpolation function, which we restate here:

$$\mu_s(x) = \frac{x}{\sqrt{1+x^2}}. \quad (3.20 \text{ revisited})$$

Now equation 5.27 becomes:

$$F = \frac{\frac{f}{a_0}}{\sqrt{1+\left(\frac{f}{a_0}\right)^2}}f. \quad (5.28)$$

Rewriting this, we obtain:

$$f^4 - F^2 f^2 - a_0^2 F^2 = 0. \quad (5.29)$$

Solving this for f^2 we obtain:

$$f^2 = \frac{1}{2}F^2 \pm \frac{1}{2}F\sqrt{F^2 + 4a_0^2}. \quad (5.30)$$

We want $f > F$ (remember that F corresponds to the Newtonian acceleration and f to the actual acceleration) to obtain the higher velocities observed compared to the Newtonian prediction, so we choose addition in this formula. Finally:

$$f = F\sqrt{\frac{1}{2} + \frac{1}{2}\sqrt{1 + 4\frac{a_0^2}{F^2}}}, \quad (5.31)$$

or

$$\mathbf{f} = \sqrt{\frac{1}{2} + \frac{1}{2}\sqrt{1 + 4\frac{a_0^2}{F^2}}}\mathbf{F}. \quad (5.32)$$

In general we then have

$$f = v\left(\frac{F}{a_0}\right)F, \quad (5.33)$$

in which $v(y)$ is the inverse relation of a certain interpolation function $\mu(x)$ with $y = \frac{F}{a_0}$.

Now we state the inverse interpolation function $v(y)$ for the other 2 interpolation functions $\mu_\nu(x)$ and $\mu_{\text{angus}}(x)$ mentioned in section 3:

$$v_\nu(y) = \frac{y + \sqrt{y}}{y}. \quad (5.34)$$

$$v_{\text{angus}}(y) = \frac{1}{2} + \frac{1}{2}\sqrt{1 + \frac{4}{y}}. \quad (5.35)$$

5.4.2. The iterative method

Now we summarize this section in a system of equations:

$$-\nabla \cdot \mathbf{a}_N = 4\pi G\rho \quad (2.14 \text{ revisited})$$

$$\mathbf{F} = \mathbf{a}_N + \mathbf{B} \quad (5.36)$$

$$\mathbf{F} = \mu\left(\frac{|\mathbf{f}|}{a_0}\right)\mathbf{f} \quad (5.27 \text{ revisited})$$

$$\mathbf{f} = v\left(\frac{F}{a_0}\right)\mathbf{F} \quad (5.33 \text{ revisited})$$

$$\nabla \cdot \mathbf{B} = 0 \quad (5.37)$$

$$\nabla \times \mathbf{f} = 0 \quad (5.38)$$

This system of equations can not be solved analytically for \mathbf{f} , however, it can be solved with an iterative approach proposed by Dr. P.M. Visser. We define sequences \mathbf{f}_n , \mathbf{B}_n and \mathbf{F}_n with $n = 0, 1, 2, \dots$. The iterative process starts by setting $\mathbf{B}_0 = 0$, so equation 5.36 gives:

$$\mathbf{F}_0 = \mathbf{a}_N + \mathbf{B}_0. \quad (5.39)$$

Then we can use equation 5.33:

$$\mathbf{f}_0 = \nu \left(\frac{F_0}{a_0} \right) \mathbf{F}_0. \quad (5.40)$$

This is the zeroth order approximation. We know that \mathbf{f} should satisfy $\nabla \times \mathbf{f} = 0$. So we take the curl free part of \mathbf{f}_0 using the Helmholtz decomposition and Fourier transform, which results in

$$\tilde{\mathbf{f}}_1 = \tilde{\mathbf{f}}_{0,\parallel} = \frac{\mathbf{k} \cdot \tilde{\mathbf{f}}_0}{\mathbf{k} \cdot \mathbf{k}} \mathbf{k}. \quad (5.41)$$

Taking the inverse Fourier transform then and equation 5.27, we obtain:

$$\mathbf{F}_1 = \mu \left(\frac{f_{1,\parallel}}{a_0} \right) \mathbf{f}_{1,\parallel}. \quad (5.42)$$

Now with equation 5.36, we can find \mathbf{B}_1 :

$$\mathbf{B}_1 = \mathbf{F}_1 - \mathbf{a}_N. \quad (5.43)$$

However we also had as requirement that $\nabla \cdot \mathbf{B} = 0$, so for \mathbf{B}_2 we take the divergence free part using the Helmholtz decomposition and Fourier transforms:

$$\tilde{\mathbf{B}}_2 = \tilde{\mathbf{B}}_{1,\perp} = \tilde{\mathbf{B}}_1 - \frac{\mathbf{k} \cdot \tilde{\mathbf{B}}_1}{\mathbf{k} \cdot \mathbf{k}} \mathbf{k}. \quad (5.44)$$

Again taking the inverse Fourier transform and 5.36, we obtain:

$$\mathbf{F}_2 = \mathbf{a}_N + \mathbf{B}_2. \quad (5.45)$$

Using equation 5.33 again, we find the second order approximation of \mathbf{f} :

$$\mathbf{f}_2 = \nu \left(\frac{F_2}{a_0} \right) \mathbf{F}_2. \quad (5.46)$$

Now we repeat the steps above until \mathbf{f} converges. There is no guarantee that \mathbf{f} does converge, however if it converges, we know we found a solution to the system of equations. Furthermore notice that for n is odd, the n th order approximations satisfies $\nabla \times \mathbf{f}_n = 0$ and for n is even, the n th order approximations satisfies $\nabla \cdot \mathbf{B}_n = 0$.

5.5. Apparent mass distribution and apparent dark matter distribution

Using the iterative method we can find the MOND potential ϕ_M . With this known potential, it is possible to obtain the apparent mass distribution ρ_{AP} that would create such a potential with Newtonian gravity. This can be done by substituting Φ_M into the Poisson equation. Using Fourier transforms, it can be obtained with the following formula:

$$\rho_{AP} = -\mathcal{F}^{-1} \left\{ \frac{\mathbf{k} \cdot \mathbf{k} \mathcal{F}\{\phi_M\}}{4\pi G} \right\}. \quad (5.47)$$

By subtracting the actual mass density from ρ_{AP} , we can also find the apparent dark matter density $\rho_{\text{apparentDM}}$.

6

Comparison between ND and MOND on a Bullet-like cluster

In this section, the MOND potential will be calculated for a Bullet-like cluster generated as described in section 5 for the standard interpolation function and the Angus interpolation function. Furthermore the apparent dark matter found from the MOND potential will be calculated and will be compared to the dark matter model described in section 4. Also it will be studied how changing the mass and number of the galaxies will influence the dark matter distribution. For this, the MOND equations with the Angus interpolation function was used.

6.1. Mass distribution of a Bullet-like cluster and Newtonian gravity

In this section we will show the mass distribution generated as described in section 5. Also the Newtonian gravitational potential Φ_N and absolute acceleration field a will be shown. The generated mass distribution will be shown as a projected surface mass density Σ in kg/m^2 , which is the mass density in kg/m^3 added up in the z -direction for all x and y coordinates. The projected surface mass density of the generated mass distribution is shown in figure 6.1.

In figure 6.2 Φ_N for this generated mass distribution is shown, which was obtained by solving the Poisson equation. The potential is shown for different z values. Also the absolute acceleration field a corresponding to this potential is shown for $z = 0$ in figure 6.3.

It can be seen in figure 6.2 that Φ_N is (almost) spherically symmetric and is therefore dominated by the intracluster gas. As can be seen in figure 6.3, the acceleration field a is below a_0 for most of the plane. Also notice that a decreases close to the center of the intracluster gas. This is expected as a result of the Shell theorem. Also for every galaxy, a becomes close to 0 close to the galaxy, between the galaxy and the center of the galaxy cluster. This result is also expected, as in that position, the gravitational pull due to the galaxy is equal to the gravitational pull of total the galaxy cluster, which results in a saddle point for the acceleration field. In figure 6.4 the dark matter surface mass density is shown corresponding to section 4 based on the paper of Paraficz et al. Notice that the range of the projected surface mass density is around a factor 2 larger for the dark matter than the actual baryonic mass. The projected baryonic mass surface density and the dark matter surface mass density together are shown in figure 6.5.

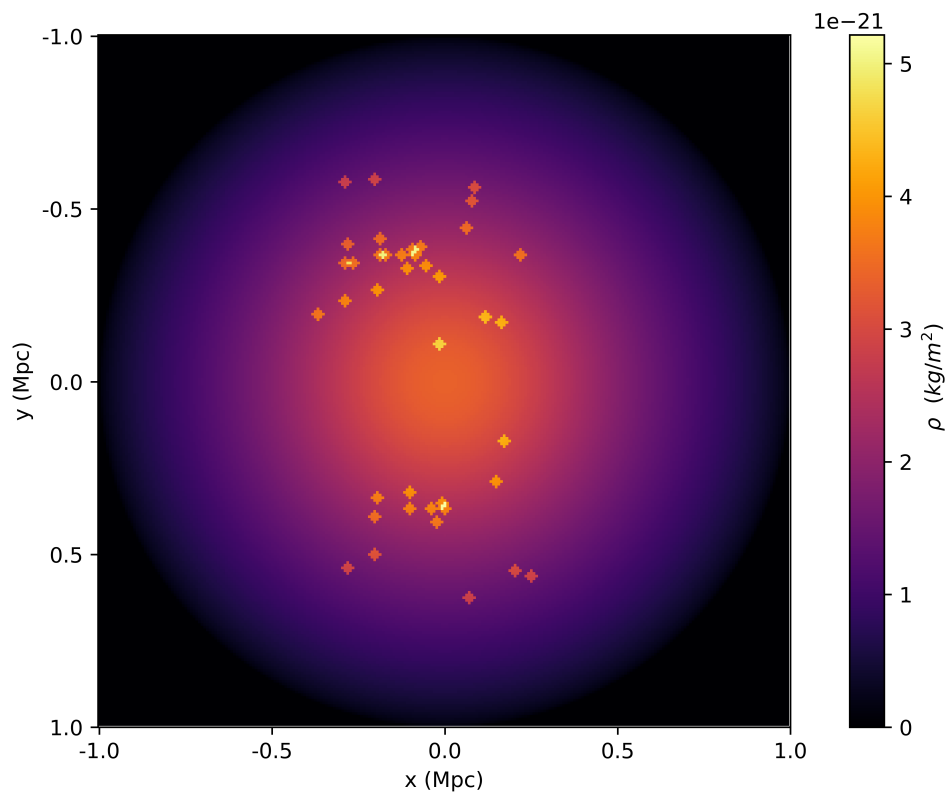


Figure 6.1: The projected baryonic mass density generated according to section 5 in kg/m^2 . The baryonic mass consists of 40 galaxies with $M = M_{\text{Milky Way}}$ and the intracluster gas.

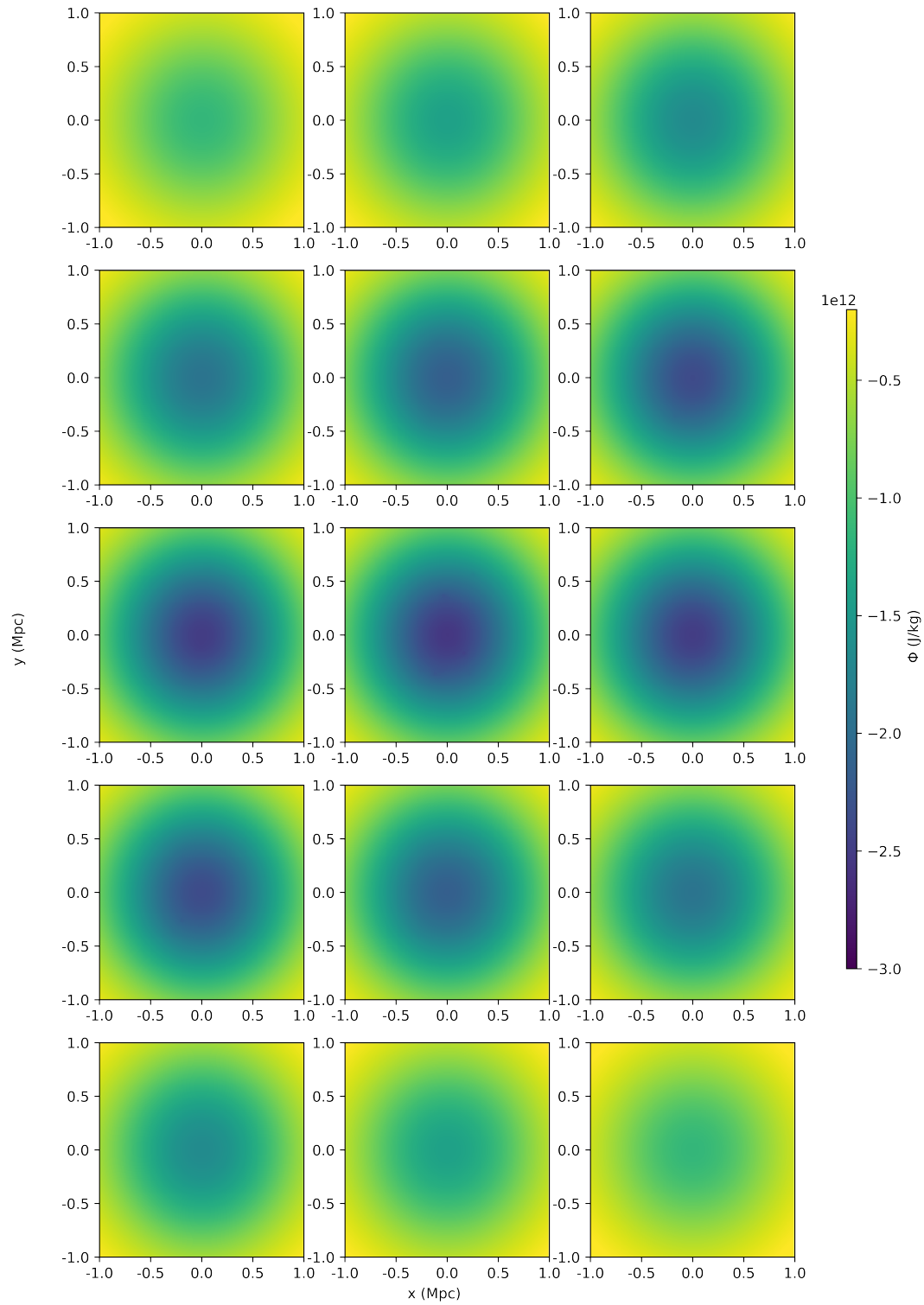


Figure 6.2: The Newtonian gravitational potential in kg/J plotted in x, y -plane for different values of z . The plots are placed at $z = \frac{2000}{256} n$ kpc with $n = -7, -6, \dots, 6, 7$ from left to right and then from above to under.

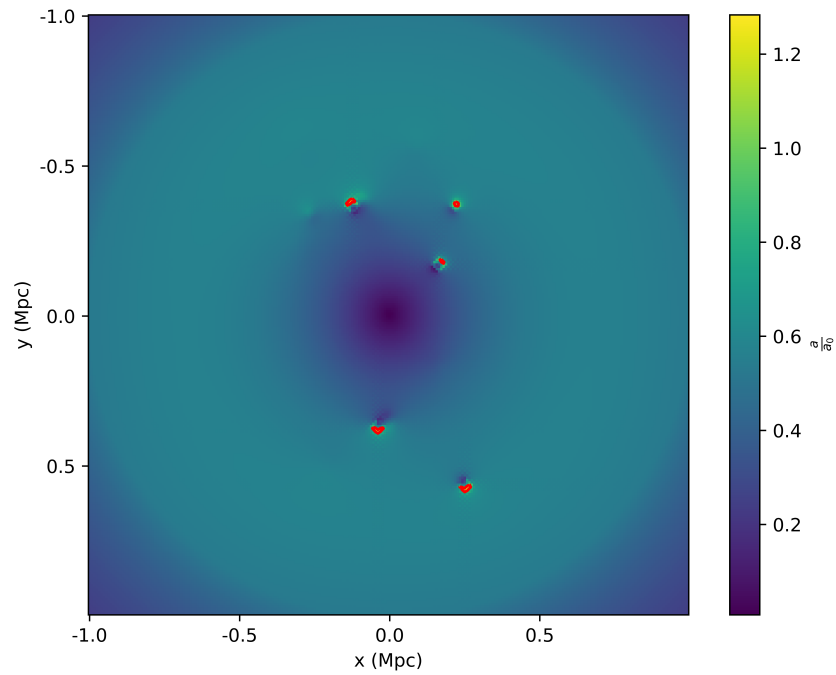


Figure 6.3: The absolute acceleration a due to the baryonic mass density taken at $z = 0$ in units a_0 . The red contours correspond to absolute accelerations equal to a_0 .

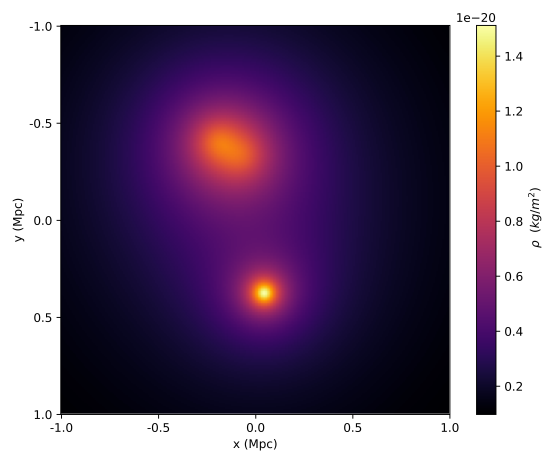


Figure 6.4: The projected dark matter surface densities from parameters found in the paper of Paraficz et al [15].

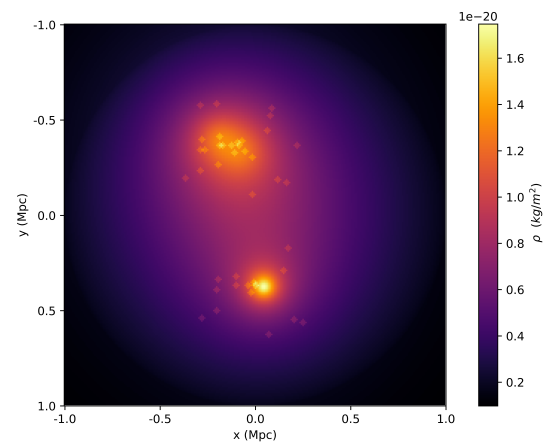


Figure 6.5: The projected dark matter surface densities from parameters found in the paper of Paraficz et al [15] added to the projected baryonic mass surface density generated with the model described in section 5.

6.2. Using MOND on the Bullet-like cluster

In this section the MOND potential was calculated as described in section 5 with the standard interpolation function and the Angus interpolation function, and both the 2nd order approximation for the iterative method. The MOND results with the Verlinde interpolation function is presented in the appendix. The absolute acceleration field f in units of a_0 is calculated and the projected apparent matter surface mass density Σ_{apparent} in kg/m^2 and the projected apparent dark matter surface mass density $\Sigma_{\text{apparentDM}}$ in kg/m^2 . We had already seen that the ND acceleration field was mostly below a_0 , but still around the order of magnitude of a_0 . This is also the range in which the interpolation functions differ in behaviour as could be seen in figure 3.1, so we should expect different potentials and apparent matter distributions.

6.2.1. Standard interpolation

In figure 6.6 the MOND potential $\Phi_{M,s}$ using the standard interpolation function is presented for different z coordinates. In figure 6.7 the absolute acceleration field f_s derived from the MOND potential using the standard interpolation function are plotted in the x, y -plane for the value $z = 0$.

Comparing figures 6.6 and 6.2, we can see that $\Phi_{M,s}$ is steeper than Φ_N (note the different scale). In both potentials the intracluster gas seems to dominate the potential, as the galaxies are not visible in the potential. Also by comparing figures 6.7 and 6.3, we can see that the acceleration field f_s is generally higher than the field a . For the Newtonian gravitational acceleration field a , only close to the galaxies does it reach a_0 . Also f_s is larger than a_0 only close to the galaxies, but for a larger area. The increase in the acceleration field is expected, as MOND should add 'dark matter' to the baryonic matter for the acceleration field below a_0 and increase the field.

In figure 6.8 the projected apparent matter mass density due to the MOND potential of the standard interpolation is shown. Also the projected apparent dark matter mass density is shown in 6.9

Comparing figures 6.8 and 6.1, the mass distributions seem to resemble each other except for the absolute value of the densities. Comparing figures 6.9 and 6.4, the mass distributions do not seem to be equivalent. The projected apparent dark matter density has dark matter concentrated in the center of the intracluster gas and the apparent dark matter does not seem to spatially coincide with the galaxies. Also the projected dark matter density is significantly lower than the deduced dark matter distribution.

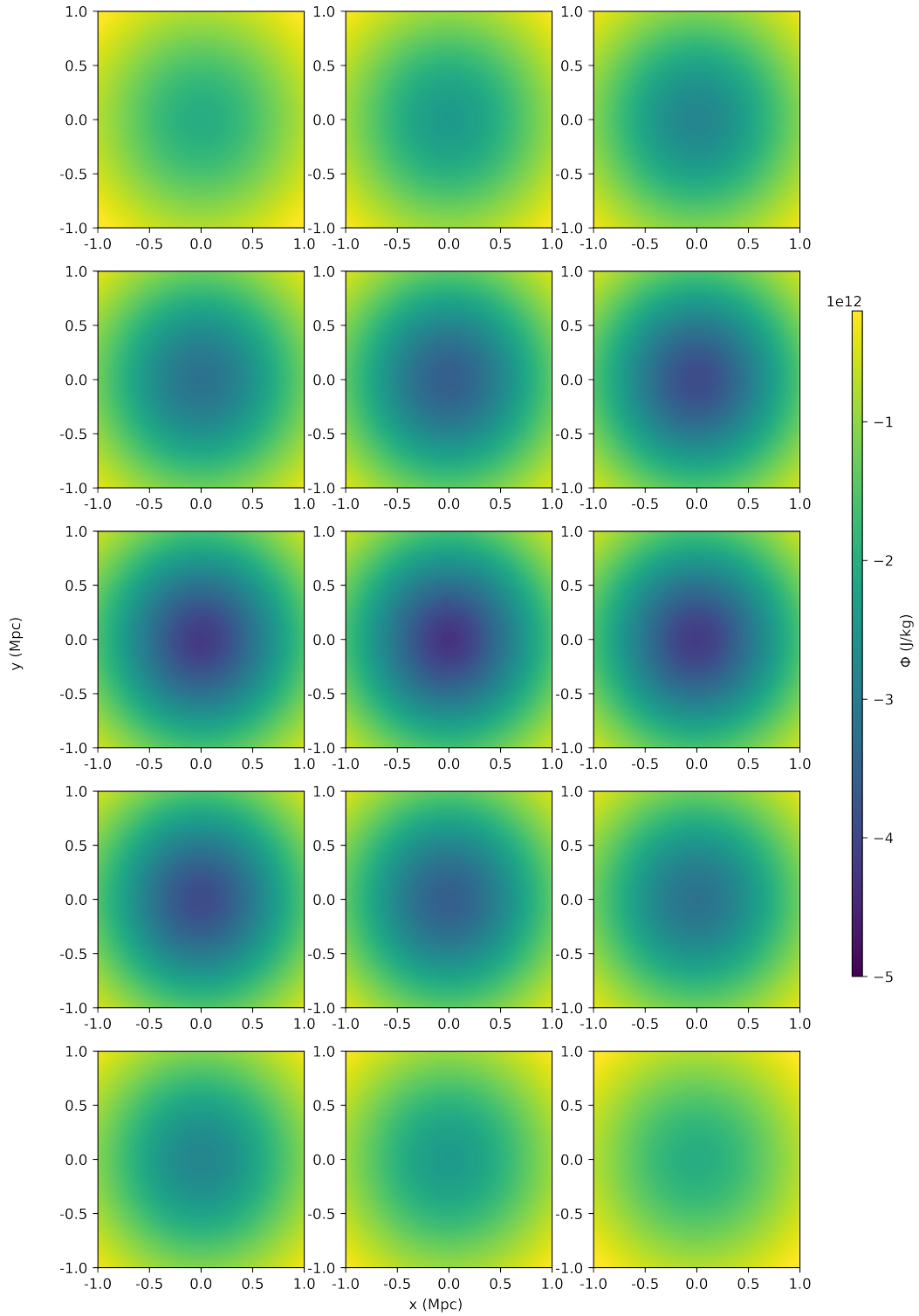


Figure 6.6: Gravitational potential using MOND $\Phi_{M,s}$ with the standard interpolation function plotted in x, y -plane for different values of z . The plots are located at $z = \frac{2000}{256} n$ kpc with $n = -7, -6, \dots, 6, 7$ from left to right and then from above to under.

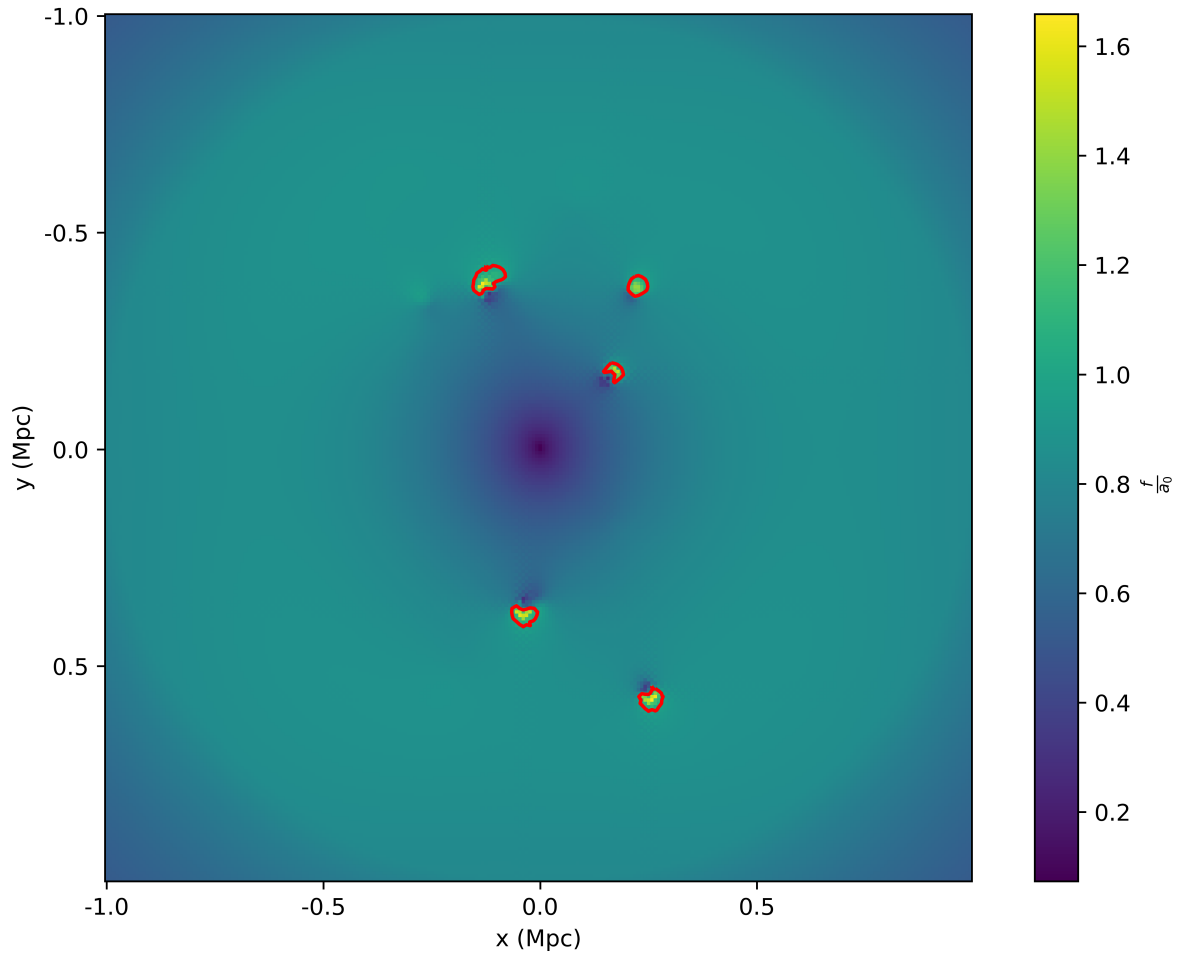


Figure 6.7: The absolute acceleration f_s derived from the MOND potential with the standard interpolation function taken at $z = 0$ in units of a_0 . The red contours correspond to absolute accelerations equal to a_0 .

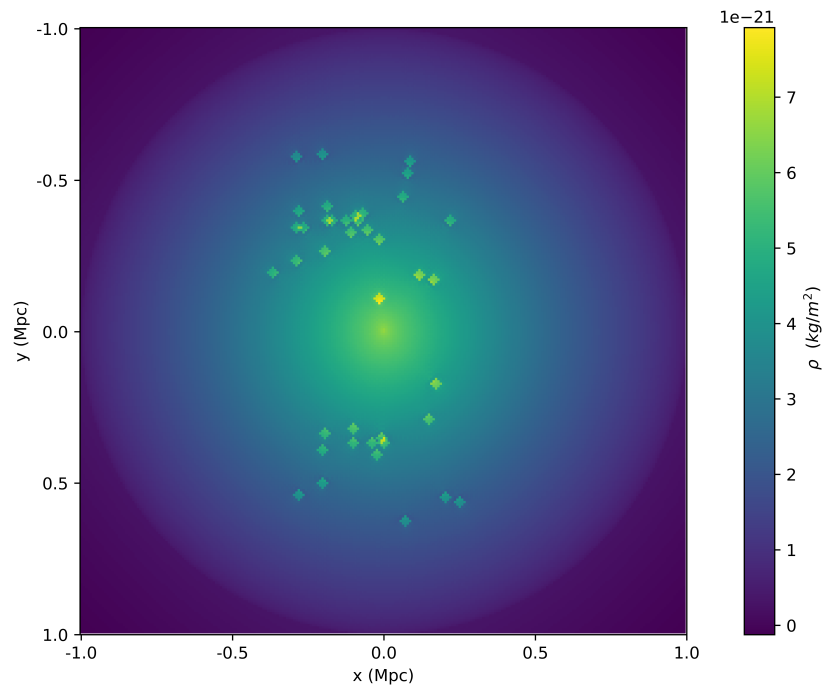


Figure 6.8: The projected apparent matter density calculated using MOND with the standard interpolation function.

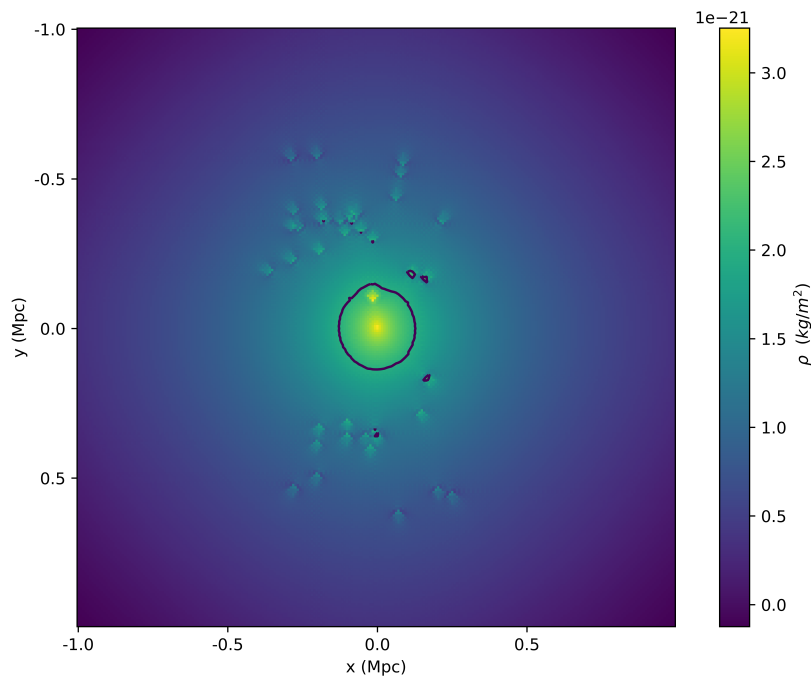


Figure 6.9: The projected apparent dark matter density calculated using MOND with the standard interpolation function. The apparent dark matter is obtained by subtracting the baryonic matter from the apparent matter. The black contour correspond to $\Sigma_{\text{apparentDM}} = 2 \cdot 10^{-21} \text{ kg/m}^2$ and the yellow contours correspond to $\Sigma_{\text{apparentDM}} = 4 \cdot 10^{-21} \text{ kg/m}^2$.

6.2.2. MOND with Angus interpolation

In figure 6.10 the MOND potential $\Phi_{M,a}$ of the Angus interpolation is presented for different z coordinates. In figure 6.11 the absolute acceleration field f_a are plotted in the x, y -plane for the value $z = 0$.

Comparing $\Phi_{M,a}$ with the potentials using the other interpolation functions, we see that it is similar, but $\Phi_{M,s}$ is less steep. The absolute acceleration field f_a is much higher than the Newtonian acceleration field a and f_s . As can be seen in figure 6.11, f_a is higher than a_0 mostly in the Bullet-like cluster, except far from the center and close to the center. This corresponds to the Shell theorem. The red contours in figure close to galaxies between the 2 large contours correspond to areas in which the acceleration is below a_0 . These are the saddle points mentioned before.

In figure 6.12 the projected apparent matter mass density derived from $\Phi_{M,a}$ is shown. Also the projected apparent dark matter mass density is shown in 6.13

By comparing figures 6.12 and 6.1, we see again that the mass distribution seems to resemble each other except for the absolute value of the densities. By looking at figure 6.13, we can see that the apparent dark matter is still distributed almost spherically symmetric and concentrated at the center of the intracluster gas. Comparing figures 6.13 and 6.9, shape of the distributions are similar, however the Angus interpolation results in more dark matter. This is also in accordance with the fact that $\Phi_{M,a}$ is steeper $\Phi_{M,s}$ and that the standard interpolation function converges faster to 1 than the Angus interpolation function. In figure 6.14, the projected apparent dark matter densities of MOND equations with the standard interpolation function and the Angus interpolation function are repeated next to the projected dark matter density obtained from the paper of Paraficz et al.

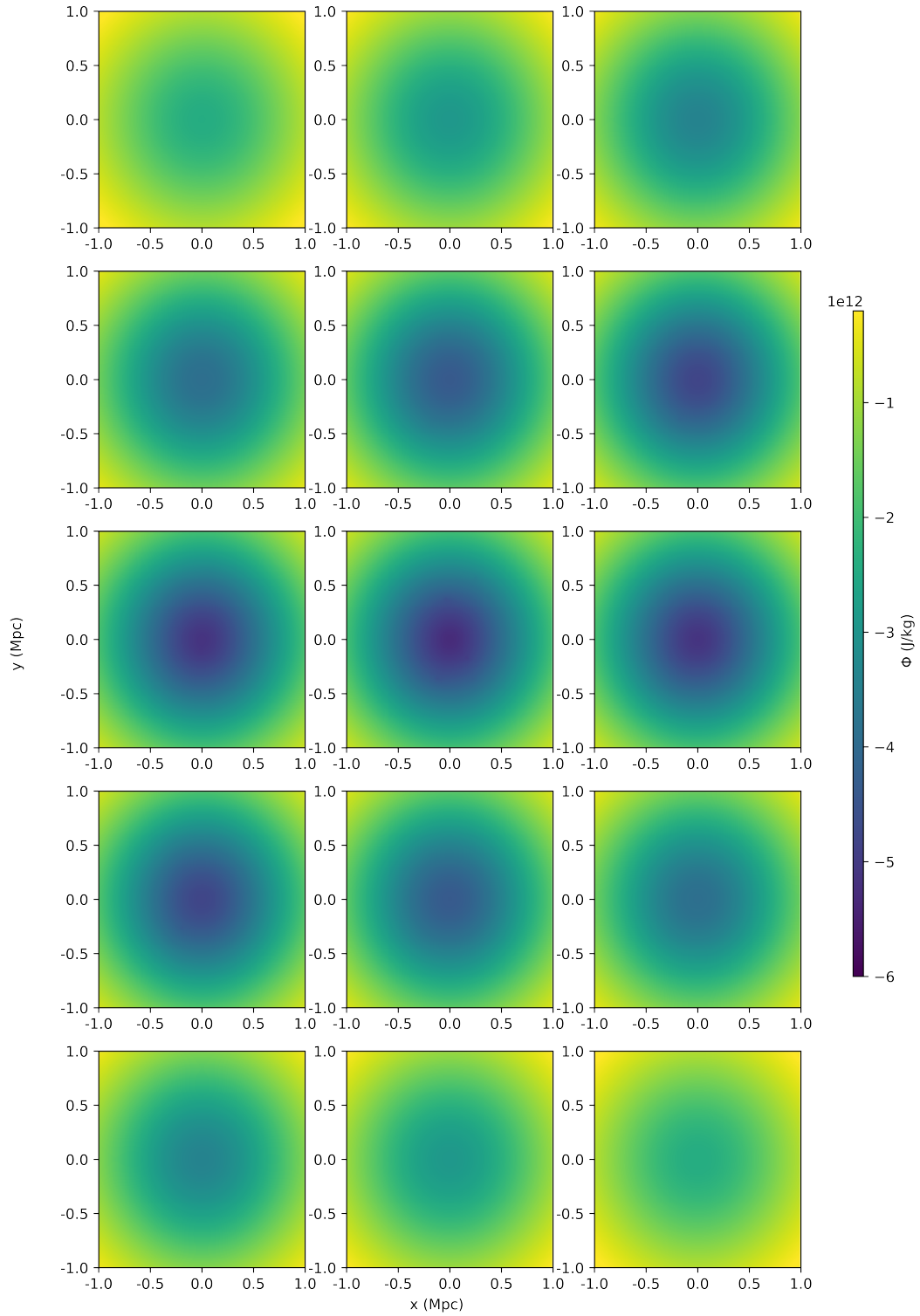


Figure 6.10: Gravitational potential using MOND with the Angus interpolation function plotted in x, y -plane for different values of z . The plots are located at $z = \frac{2000}{256} n$ kpc with $n = -7, -6, \dots, 6, 7$ from left to right and then from above to under.

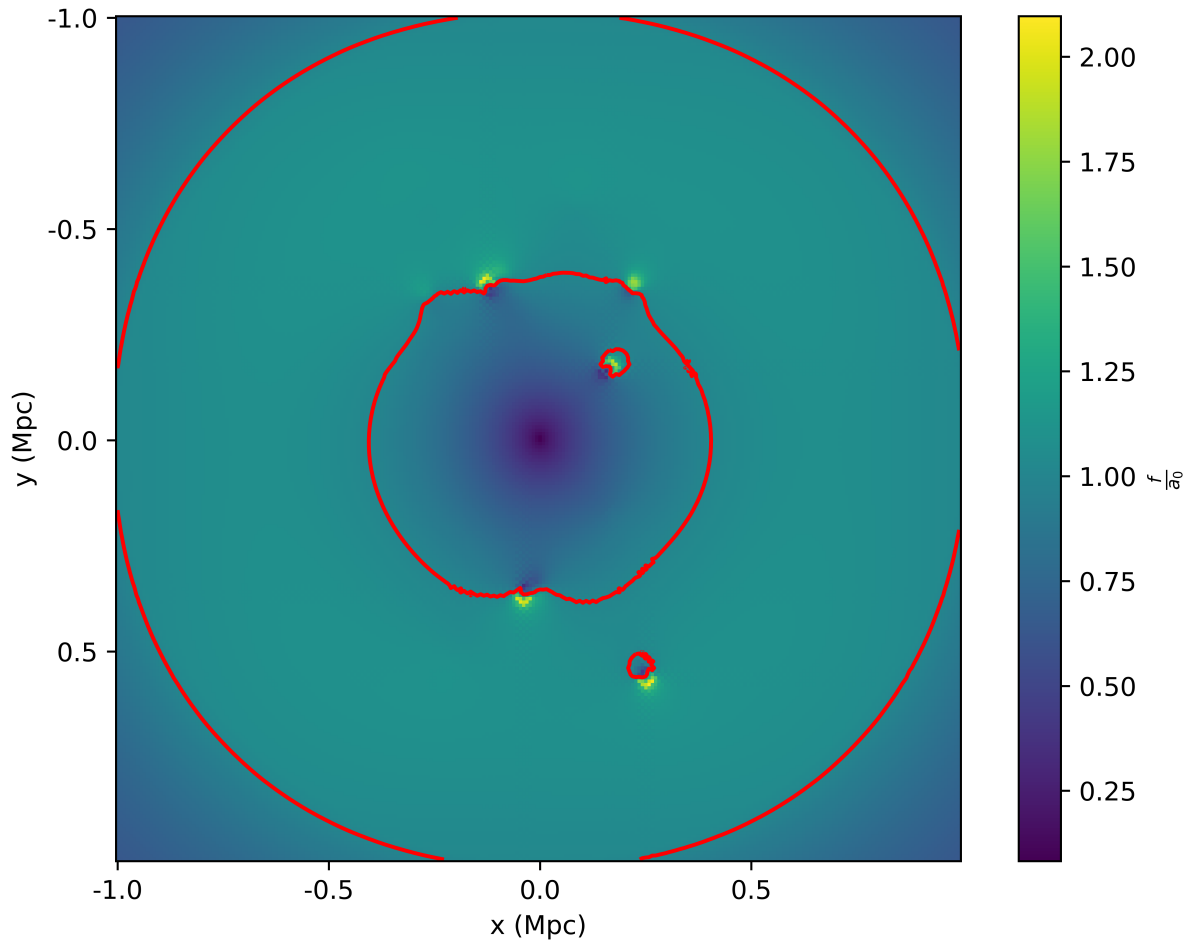


Figure 6.11: The absolute acceleration due to the MOND potential with the Angus interpolation function taken at $z = 0$ in units of a_0 . The red contours correspond to absolute accelerations equal to a_0 .

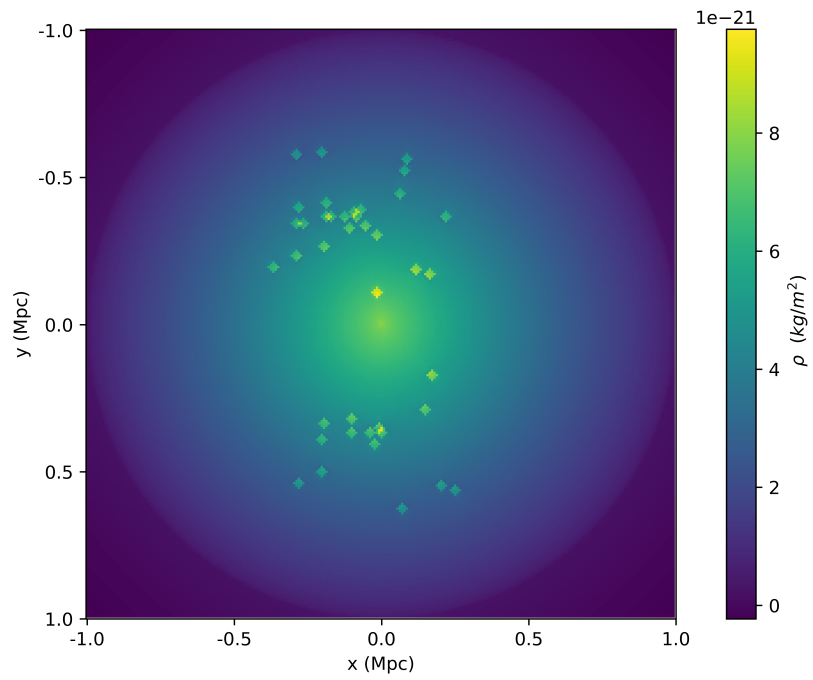


Figure 6.12: The projected apparent matter density calculated using MOND with the Angus interpolation function.

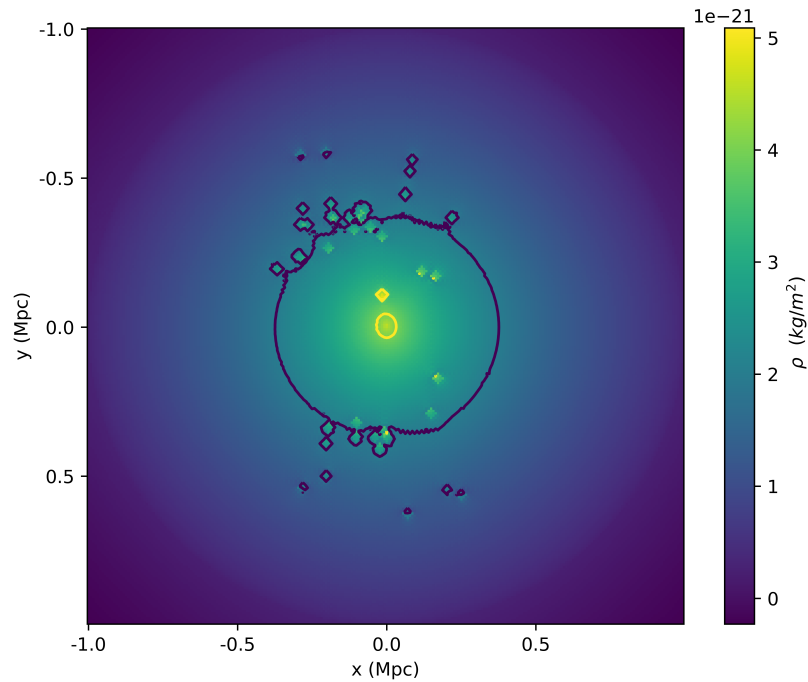


Figure 6.13: The projected apparent dark matter density using MOND with the Angus interpolation function. The apparent dark matter is obtained by subtracting the baryonic matter from the apparent matter. The black contour correspond to $\Sigma_{\text{apparentDM}} = 2 \cdot 10^{-21} \text{ kg/m}^2$ and the yellow contours correspond to $\Sigma_{\text{apparentDM}} = 4 \cdot 10^{-21} \text{ kg/m}^2$.

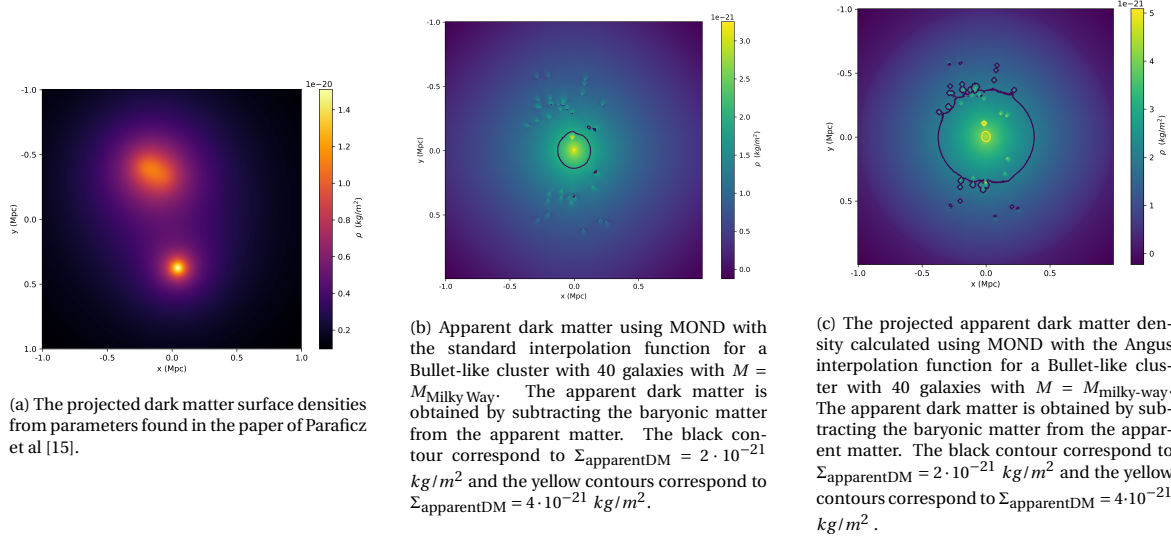


Figure 6.14: A comparison between the projected dark matter surface densities using MOND with different interpolation functions and the projected dark matter surface density found using the parameters found in the paper of Paraficz et al.

6.3. Changing the mass of the galaxies

In the previous section we have studied MOND with the different interpolation functions. The Angus and standard interpolation functions result in similar apparent matter distributions, but differ in magnitude. In this section we will study the effect of changing the mass of the galaxies in the Bullet-like cluster on the shape of the MOND potential and the apparent dark matter distributions using the Angus interpolation function. We will study the projected apparent dark matter mass distribution when the galaxies have mass $M = 10 \cdot M_{\text{Milky-way}}$ and when they have mass $M = 50 \cdot M_{\text{Milky-way}}$

In figure 6.15b the projected apparent dark matter mass density is shown for galaxies with $M = 10 \cdot M_{\text{Milky-way}}$ and in figure 6.15c for galaxies 50 with $M = 50 \cdot M_{\text{Milky-way}}$.

Comparing the projected apparent dark matter mass density for the different galaxy masses, we see that for galaxies with $M = 10 \cdot M_{\text{Milky-way}}$, the apparent dark matter is located evenly around the center of the intracluster gas and the galaxies. For galaxies with $M = 50 \cdot M_{\text{Milky-way}}$ the dark matter is mostly spatially coinciding with the galaxies. The absolute value of the dark matter close to the center of the galaxy cluster remains the same size. The projected mass density map for galaxies with $M = 50 \cdot M_{\text{Milky-way}}$ is most similar to figure 6.15d.

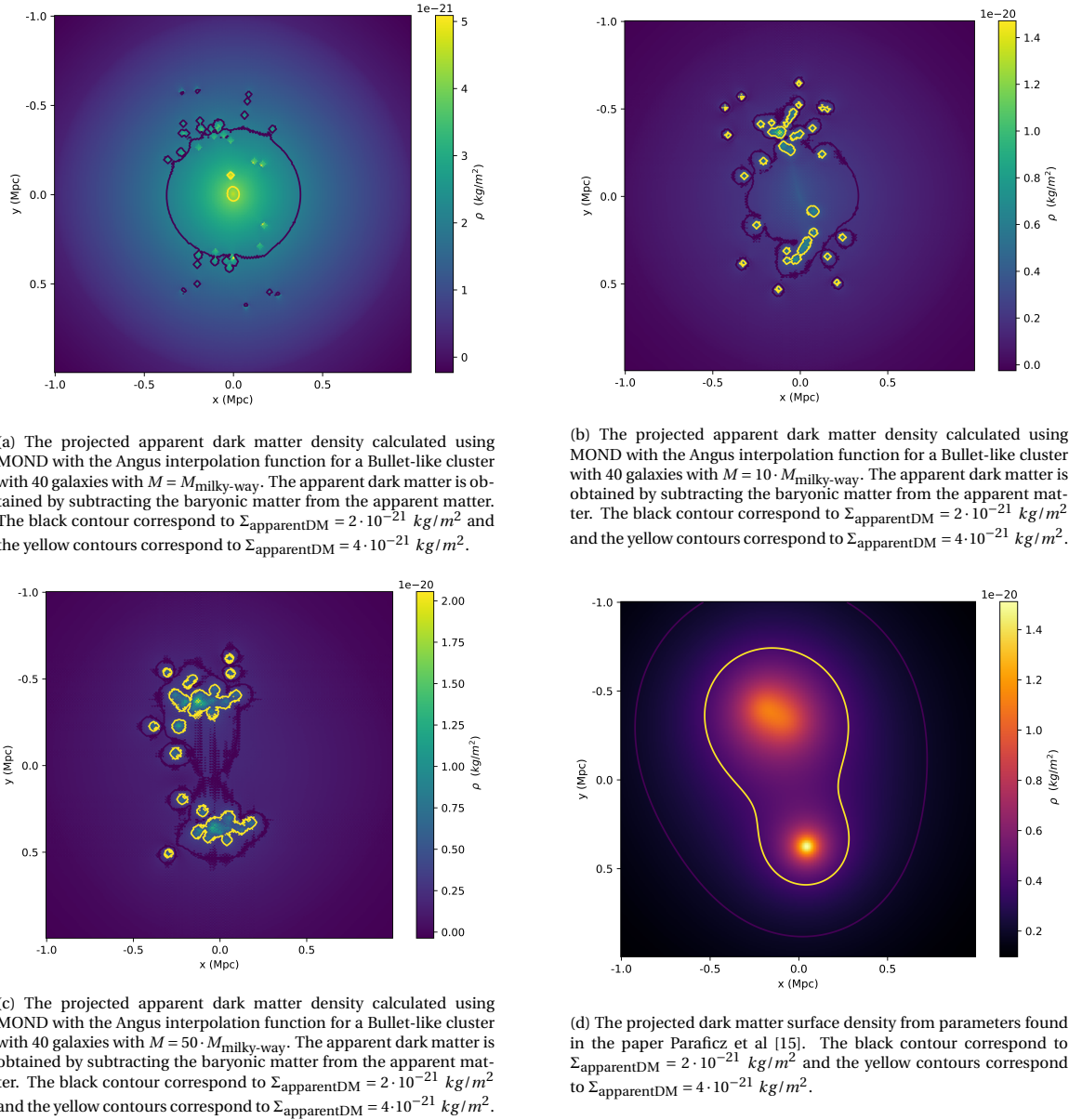


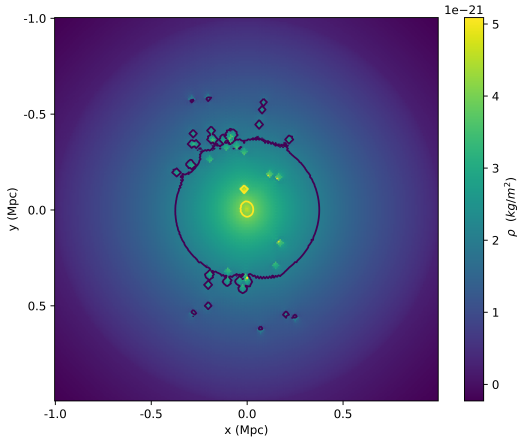
Figure 6.15: A comparison between the projected dark matter surface densities calculated using MOND with different number of galaxies with mass $M = 1.26 \cdot 10^{11} M_{\odot}$.

6.4. Changing the number of the galaxies

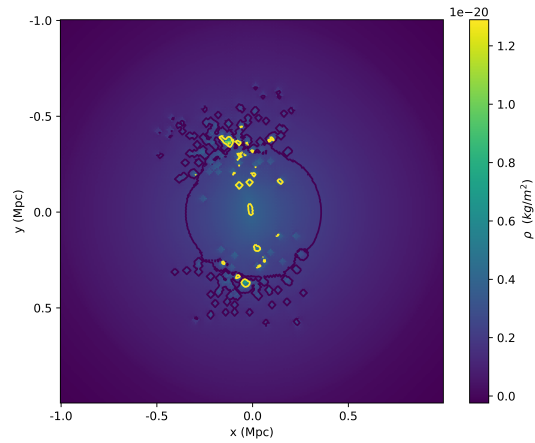
In this section we will study the effect of changing the number of the galaxies in the Bullet-like cluster on the shape of the MOND potential and the apparent dark matter distributions using the Angus interpolation function. The ratio of galaxies between the main and sub cluster will remain constant for the number of galaxies. We will study the projected apparent dark matter mass distribution when we increase the number of galaxies by 5 and by 20, so 200 galaxies and 800 galaxies respectively.

In figure 6.16b the projected apparent dark matter mass density is shown for a Bullet-like cluster with 5 times as many galaxies and in figure 6.16c the projected apparent dark matter mass density is shown for a Bullet-like cluster with 20 times as many galaxies.

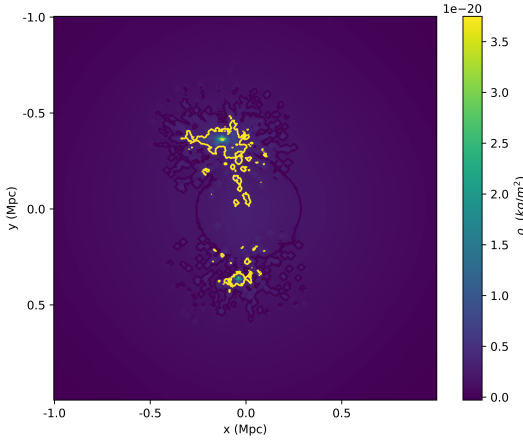
Comparing the projected apparent dark matter mass density for the different number of galaxies, we see that the dark matter is still located closer to the center of the intracluster gas for an increase of galaxies by 5. For an increase of galaxies by 20 we start to see that the apparent dark matter coincides the galaxies.



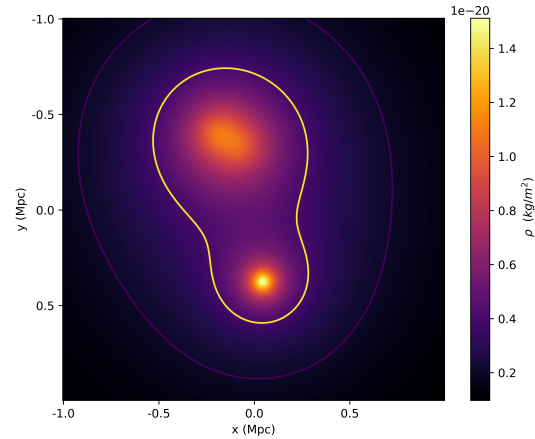
(a) The apparent dark matter density calculated using MOND with the Angus interpolation function for a Bullet-like cluster with 40 galaxies. The apparent dark matter is obtained by subtracting the baryonic matter from the apparent matter. The black contour correspond to $\Sigma_{\text{apparentDM}} = 2 \cdot 10^{-21} \text{ kg/m}^2$ and the yellow contours correspond to $\Sigma_{\text{apparentDM}} = 4 \cdot 10^{-21} \text{ kg/m}^2$.



(b) The apparent dark matter density calculated using MOND with the Angus interpolation function for a Bullet-like cluster with 200 galaxies. The apparent dark matter is obtained by subtracting the baryonic matter from the apparent matter. The black contour correspond to $\Sigma_{\text{apparentDM}} = 2 \cdot 10^{-21} \text{ kg/m}^2$ and the yellow contours correspond to $\Sigma_{\text{apparentDM}} = 4 \cdot 10^{-21} \text{ kg/m}^2$.



(c) The projected apparent dark matter density calculated using MOND with the Angus interpolation function for a Bullet-like cluster with 800 galaxies. The apparent dark matter is obtained by subtracting the baryonic matter from the apparent matter. The black contour correspond to $\Sigma_{\text{apparentDM}} = 2 \cdot 10^{-21} \text{ kg/m}^2$ and the yellow contours correspond to $\Sigma_{\text{apparentDM}} = 4 \cdot 10^{-21} \text{ kg/m}^2$.



(d) The projected dark matter surface density from parameters found in the paper Paraficz et al [15]. The black contour correspond to $\Sigma_{\text{apparentDM}} = 2 \cdot 10^{-21} \text{ kg/m}^2$ and the yellow contours correspond to $\Sigma_{\text{apparentDM}} = 4 \cdot 10^{-21} \text{ kg/m}^2$.

Figure 6.16: A comparison between the projected dark matter surface densities using MOND with different number of galaxies with mass $M = M_{\text{milky-way}}$.

7

Discussion of the results

In this section the results and methods in this thesis will be discussed. A model has been made for Bullet-like cluster. We have computed the Newtonian gravitational potential Φ_N for the generated mass distribution and the various MOND potentials Φ_M using the standard interpolation function, the Verlinde interpolation function and the Angus interpolation function. From these MOND potentials, the absolute acceleration field f was calculated and shown and finally the projected apparent matter distributions and projected apparent dark matter distributions derived from the MOND potentials were presented. Also the effect of changing the mass and number of the galaxies on the projected apparent dark matter distributions has been studied.

In figure 6.1 we can see that there are two distinct clusters. In this thesis the number of galaxies in the main and sub cluster was taken to be 25 and 15, which was estimated based on the fact that the main cluster had more deduced dark matter than the sub cluster and therefore should be heavier. Furthermore we sought a physical manner to obtain a mass distribution in the radial direction of the main and sub cluster, so based on the mass distribution of a gas cloud, a radial distribution function was made. We chose r_{cutoff} to be around 300 kpc for the clusters so that the main and sub cluster remained distinct and on basis of figure 4.1. This figure is an astrophysical image of the Bullet Cluster, which presents experimental apparent mass distribution plots. Here r_c was chosen small such that the galaxies had more chance to be on the outer radius of the cluster. These choices for the generation of a Bullet-like cluster are not based on strong evidence, but changing these parameters does not result in significantly different results. Also all galaxies were chosen to have the baryonic mass of the Milky Way as it was assumed that the Milky Way is an average weighing galaxy. The intracluster gas weighs in total 100 times more than the galaxies. It was mentioned before that the intracluster gas should weigh around 10 times more than the galaxies, however the total mass of galaxies also includes dark matter which is also around 10 times heavier than the baryonic mass in the galaxy. It was not clear whether the baryonic mass of galaxies was taken or the total mass of the galaxies for the statement that the intracluster gas is around 10 times heavier than the galaxies, so it was assumed the total mass of the galaxies was taken. This assumption is based on the fact that these papers assume the dark matter model.

The analysis using ND results in expected behaviour. The calculated potential Φ_N is not influenced much by the galaxies, because the mass of the galaxies is significantly lower than the total mass of the intracluster gas. The acceleration field in the Bullet-like cluster was mostly below a_0 , but still in the order of magnitude of a_0 . This meant that the different interpolation functions mattered as in figure 3.1, we see that the interpolation functions have already significantly different values at accelerations of half a_0 . We notice that interpolation functions that converge faster to 1 have less steep MOND potentials and all the MOND potentials are steeper than Φ_N . This also results in a higher absolute acceleration field f and a higher projected apparent dark matter distribution. The Verlinde interpolation function was not presented in section 6, but was added in the appendix. The interpolation function resulted in a probable MOND potential, however the acceleration field and apparent dark matter derived from this potential was physically improbable. The images contained many large oscillations on small scales (see figures A.2 and A.4). The order of magnitude of the apparent matter was also higher by a factor of 2. Taking the 2nd order approximation for the MOND equation using the Verlinde interpolation function and calculating the divergence of f_2 and curl of B_2 , we see that both the curl and divergence are close to zero with absolute values all below order of magnitude 10^{-31} . This means

that the solution obtained with the Verlinde interpolation function in this thesis does satisfy the system of equations for MOND. The obtained physical improbable solutions are most likely the result of a mistake in the code. But if it is not, it could lead to some interesting research questions: Do the MOND equations have a unique solution to which it converges? And can you modify an interpolation function in such a way that it can create a certain mass distribution?

When using the Angus interpolation function, the effect of changing the mass and number of the galaxies was studied. In both cases, by adding more mass to the galaxy component of the cluster, the dark matter was more spatially coincident with the galaxies. This is expected as the apparent dark matter seems to be added where most mass is. Because the MOND equation is non linear, the expected result was not certain, but using this method it seems to be the case. Because the current observations show that the baryonic mass is mostly located at the intracluster gas, this means that the Bullet Cluster should have most dark matter around the gas cloud, which was specifically not the case for the Bullet Cluster. Also we looked at setting the mass of a galaxy at 10 times the baryonic mass, which is the virial mass of the Milky Way. In this case, the galaxies were a tenth of the total mass of the intracluster gas and it can be seen that even though the dark matter is still located mostly around the intracluster gas, the largest densities of the apparent dark matter are found around the galaxies.

With the assumptions made in this thesis about the Bullet Cluster, MOND seems to result in a different mass distribution than observed and the dark matter model. However a few things should be noted. The mass of galaxies was chosen to be a tenth of the virial mass of the Milky Way, so that only the baryonic mass was included. This, however, resulted in the total mass of the galaxies being 100 times smaller than the mass of the intracluster gas, which is contrary to what most papers state. By taking the virial mass of the Milky Way, the mass of the galaxies does correspond to the literature. So in this thesis it is assumed that for the mass of the galaxies, most papers include dark matter. Using the Angus interpolation function and the virial mass of the Milky Way, the projected apparent dark matter density was still spatially mostly coincident with the center of the intracluster gas, however the largest densities were already found close to the galaxies instead of the center of the galaxy cluster. By taking the mass of the galaxies to be 5 times the virial mass of the Milky Way, the projected dark matter density started to be spatially coincident with the galaxies and not the intracluster gas. These are however large changes to the amount of baryonic matter. It would mean that a lot of baryonic matter is still not found and this would also make the dark matter model and MOND unnecessary. Also, by increasing the mass of the galaxies, we already add matter to the mass distribution and it would have the same effect as adding dark matter even without MOND.

Furthermore, in this thesis also the intracluster gas was taken as in the paper of Paraficz et al and was spherically symmetric. In figure 4.1, it can be seen however that the intracluster gas does not seem spherically symmetric. Also because the MOND equation using the Verlinde interpolation function resulted in weird behaviour, it is still the question whether the MOND equations have a unique solution for the interpolation functions.

8

Conclusions and recommendations for further research

The Bullet-like cluster generated with our model was mostly in the deep MOND regime, as the acceleration field was mostly below a_0 . It was however not much lower than a_0 , so the different interpolation functions lead to different results. We had $\Phi_{M,a}$ was steeper than $\Phi_{M,s}$. This is also in accordance with that the standard interpolation function converges faster to 1 than the Angus interpolation function.

The acceleration fields derived from the MOND potential for all interpolation functions were higher than the acceleration field derived from Φ_N . This is in accordance with our expectations, as MOND should add 'dark matter' so that the accelerations increase. The acceleration field from $\Phi_{M,v}$ was improbable, as it contained many large oscillations on small scales (see figure A.2). The acceleration fields derived from $\Phi_{M,s}$ and $\Phi_{M,a}$ were similar, but f_a was in general higher than f_s . Also f_a mostly above a_0 in the Bullet-like cluster.

For $\Phi_{M,s}$ and $\Phi_{M,a}$ the projected apparent matter distributions were similar to the projected baryonic matter distribution. For $\Phi_{M,v}$, the projected apparent matter distribution resulted in a chaotic mass distribution which might be because the iterative method is not guaranteed to converge.

The projected apparent dark matter distribution of $\Phi_{M,s}$ and $\Phi_{M,a}$ were again similar and both had most dark matter located close to the center of the intracluster gas. The galaxies' influence on the dark matter density was relatively low. This is contrary to the observations of the Bullet Cluster.

By increasing the galaxies' masses, the projected dark matter densities derived from $\Phi_{M,a}$ started to more resemble the projected dark matter density deduced in the paper of Paraficz et al. Letting the galaxies have $M = 50 \cdot M_{\text{Milky Way}}$, the dark matter was mostly spatially coincident with the galaxies. Also increasing the number galaxies had a similar effect. With 800 galaxies, the dark matter was mostly spatially coincident with the galaxies. These results are expected, as the mass density of the galaxies starts to be significantly higher than the intracluster gas. However the changes to the baryonic masses are large. This would mean that a lot of baryonic mass has still not been observed, but in that case the MOND and dark matter model would also be unnecessary.

For further research, it could be interesting to study cases in which the intracluster gas is not spherically symmetric. The foremost mass component of the baryonic mass is the intracluster gas and by choosing it to be non-spherically symmetric, it might lead to interesting MOND potentials and maybe even the deduced dark matter distribution.

Another interesting research direction might be to start from the Bullet Cluster pictures itself and use weak lensing to derive the total mass distribution of the Bullet Cluster. In the paper of Paraficz et al, the mass distributions were optimized using certain algorithms and prefixed mass distributions with free parameters. However it might be possible to numerically calculate the mass density with weak lensing without assuming a trial form for the mass distributions beforehand.

It also might be interesting to study why the MOND equations using the Verlinde interpolation function did not converge to a (probable) solution using the iterative method. Assuming no coding mistake was made, it may mean that the MOND equations do not converge to a unique solution for any interpolation function. Also it might be the case that interpolation functions can be constructed to obtain certain matter distributions.

Bibliography

- [1] Garry W Angus, Benoit Famaey, and HongSheng Zhao. Can mond take a bullet? analytical comparisons of three versions of mond beyond spherical symmetry. *Monthly Notices of the Royal Astronomical Society*, 371(1):138–146, 2006.
- [2] Jacob D Bekenstein. Black holes and the second law. In *JACOB BEKENSTEIN: The Conservative Revolutionary*, pages 303–306. World Scientific, 2020.
- [3] Maruša Bradač, Douglas Clowe, Anthony H Gonzalez, Phil Marshall, William Forman, Christine Jones, Maxim Markevitch, Scott Randall, Tim Schrabback, and Dennis Zaritsky. Strong and weak lensing united. iii. measuring the mass distribution of the merging galaxy cluster 1es 0657–558. *The Astrophysical Journal*, 652(2):937, 2006.
- [4] Margot M Brouwer, Kyle A Oman, Edwin A Valentijn, Maciej Bilicki, Catherine Heymans, Henk Hoekstra, Nicola R Napolitano, Nivya Roy, Crescenzo Tortora, Angus H Wright, et al. The weak lensing radial acceleration relation: Constraining modified gravity and cold dark matter theories with kids-1000. *arXiv preprint arXiv:2106.11677*, 2021.
- [5] Dimitris M. Christodoulou and Demosthenes Kazanas. The case against dark matter and modified gravity: Flat rotation curves are a rigorous requirement in rotating self-gravitating newtonian gaseous discs. *Journal of Modern Physics*, 7(7), 1989.
- [6] LP David, A Slyz, Ch Jones, W Forman, SD Vrtillek, and KA Arnaud. A catalog of intracluster gas temperatures. *The Astrophysical Journal*, 412:479–488, 1993.
- [7] Herbert Goldstein, Charles Poole, and John Safko. *Classical mechanics*, 2002.
- [8] Marceau Limousin, Jean-Paul Kneib, and Priyamvada Natarajan. Constraining the mass distribution of galaxies using galaxy-galaxy lensing in clusters and in the field. *Monthly Notices of the Royal Astronomical Society*, 356(1):309–322, 2005.
- [9] M Markevitch, AH Gonzalez, L David, A Vikhlinin, S Murray, W Forman, C Jones, and W Tucker. A textbook example of a bow shock in the merging galaxy cluster 1e 0657–56. *The Astrophysical Journal*, 567(1):L27, 2002.
- [10] Maxim Markevitch, AH Gonzalez, D Clowe, A Vikhlinin, W Forman, C Jones, S Murray, and W Tucker. Direct constraints on the dark matter self-interaction cross section from the merging galaxy cluster 1e 0657–56. *The Astrophysical Journal*, 606(2):819, 2004.
- [11] David Merritt. The distribution of dark matter in the coma cluster. *The Astrophysical Journal*, 313:121–135, 1987.
- [12] M Milgrom. Milgrom’s perspective on the bullet cluster. *The MOND pages*, 2016.
- [13] Mordehai Milgrom. A modification of the newtonian dynamics as a possible alternative to the hidden mass hypothesis. *The Astrophysical Journal*, 270:365–370, 1983.
- [14] Isaac Newton. *Philosophiæ naturalis principia mathematica*, volume 1. G. Brookman, 1833.
- [15] D Paraficz, J-P Kneib, J Richard, A Morandi, M Limousin, E Jullo, and Johany Martinez. The bullet cluster at its best: weighing stars, gas, and dark matter. *Astronomy & Astrophysics*, 594:A121, 2016.
- [16] Hans-Walter Rix and Jo Bovy. The milky way’s stellar disk. *The Astronomy and Astrophysics Review*, 21(1):1–58, 2013.

- [17] Vera C Rubin, W Kent Ford Jr, and Norbert Thonnard. Extended rotation curves of high-luminosity spiral galaxies. iv-systematic dynamical properties, sa through sc. *The Astrophysical Journal*, 225:L107–L111, 1978.
- [18] AS Sarabi, Varamin Pishva Branch, Iran Bijan Nikouravan, and F Abaei. Relationship between newtonian and mondian acceleration. *Advances in Applied Physics*, 4(1):31–37, 2016.
- [19] Odessa Schokker. Relating modified newtonian dynamics to dark matter - application to a virgo-like galaxy cluster, 2022.
- [20] AM Stewart. Longitudinal and transverse components of a vector field. *arXiv preprint arXiv:0801.0335*, 2008.
- [21] Virginia Trimble. Existence and nature of dark matter in the universe. *Annual review of astronomy and astrophysics*, 25(1):425–472, 1987.
- [22] W Tucker, P Blanco, S Rappoport, L David, D Fabricant, EE Falco, W Forman, A Dressler, and M Ramella. 1e 0657–56: A contender for the hottest known cluster of galaxies. *The Astrophysical Journal*, 496(1):L5, 1998.
- [23] Erik Verlinde. On the origin of gravity and the laws of newton. *Journal of High Energy Physics*, 2011(4): 1–27, 2011.
- [24] Erik Verlinde. Emergent gravity and the dark universe. *SciPost Physics*, 2(3):016, 2017.
- [25] Fritz Zwicky. Die rotverschiebung von extragalaktischen nebeln. *Helvetica physica acta*, 6:110–127, 1933.

A

MOND with the Verlinde interpolation function

In this section, MOND with the Verlinde interpolation function will be studied. In figure A.1 the MOND potential $\Phi_{M,v}$ with the Verlinde interpolation function is presented for different z coordinates. In figure A.2 the absolute acceleration field f_v is plotted in the x, y -plane for the value $z = 0$.

Comparing $\Phi_{M,s}$ and $\Phi_{M,v}$, we see that $\Phi_{M,v}$ is steeper, but the shape is similar. However the absolute acceleration field f_v has unexpected and physically improbable shape. In figure A.3 the projected apparent matter mass density due to the MOND potential of the Verlinde interpolation is shown. Also the projected apparent dark matter mass density is shown in A.4.

The projected apparent mass densities show an improbable apparent mass distribution. The Verlinde interpolation does not become less chaotic after more iterations. By calculating the divergence of f_2 and the curl of B_2 , we see that both the curl and divergence are close to zero with absolute values all below order of magnitude 10^{-31} , so the solution does satisfy the system of equations for MOND.

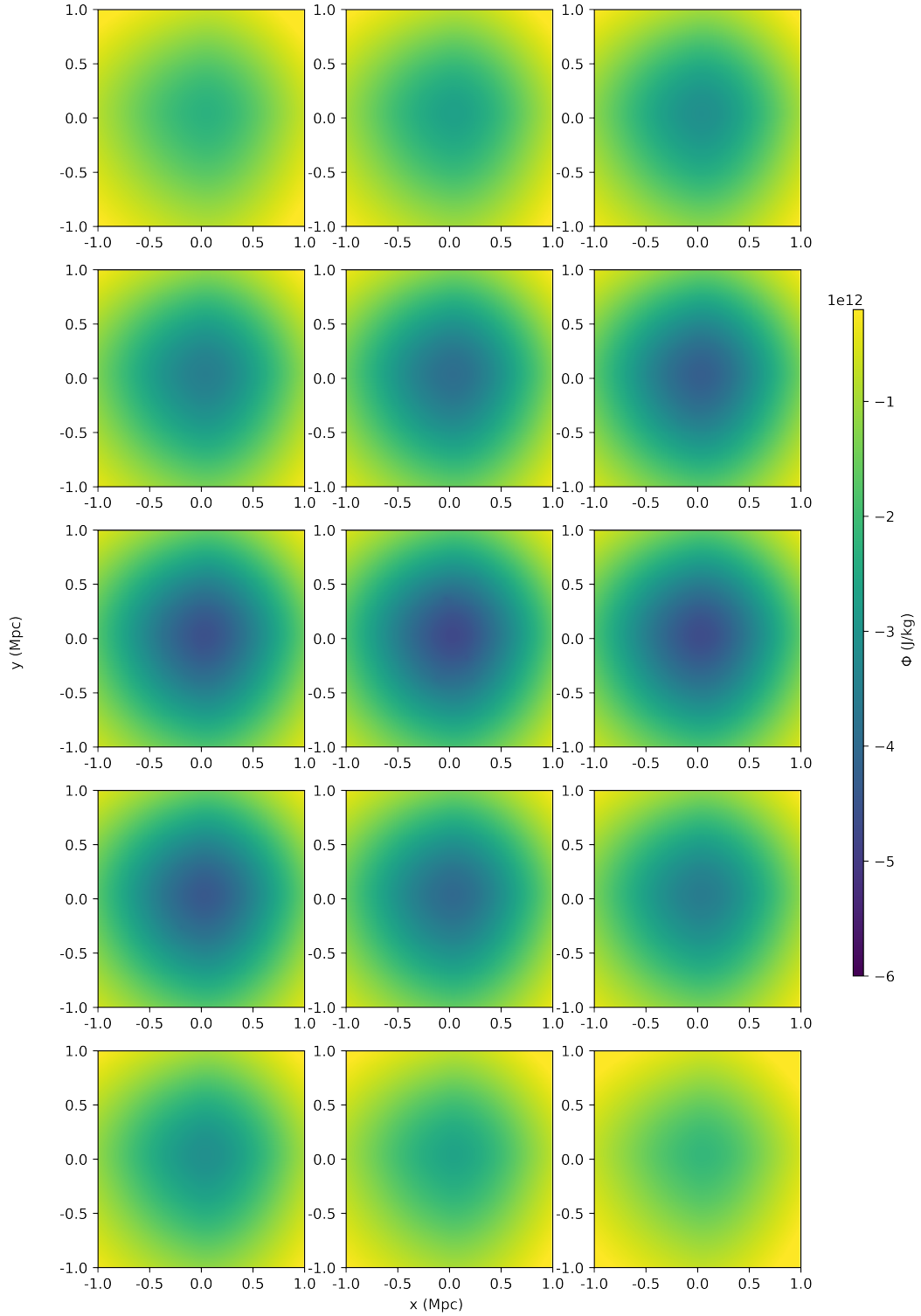


Figure A.1: Gravitational potential $\Phi_{M,v}$ using MOND with the Verlinde interpolation function plotted in x, y -plane for different values of z . The plots are located at $z = \frac{2000}{256} n$ kpc with $n = -7, -6, \dots, 6, 7$ from left to right and then from above to under.

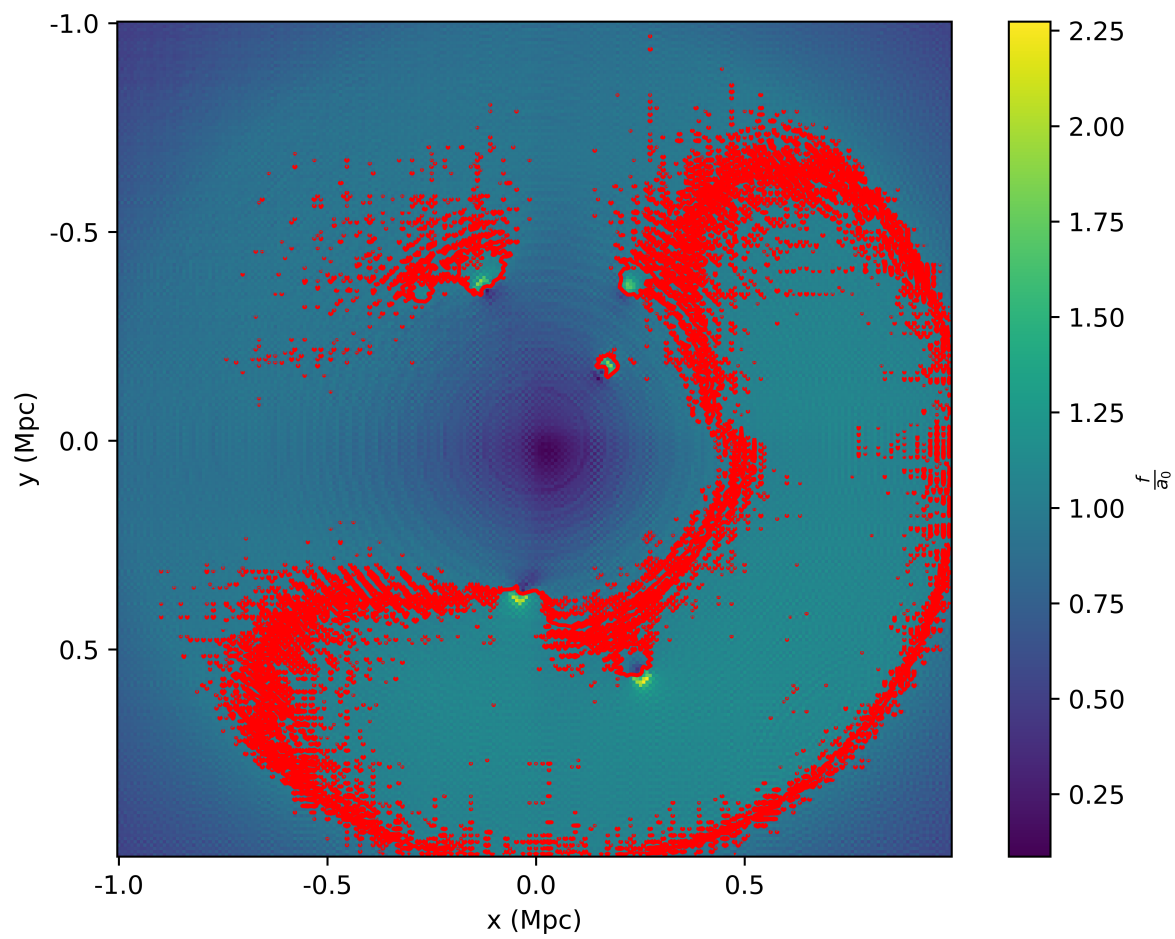


Figure A.2: The absolute acceleration field f_V due to the MOND potential with the Verlinde interpolation function taken at $z = 0$ in units of a_0 . The red contours correspond to absolute accelerations equal to a_0 .

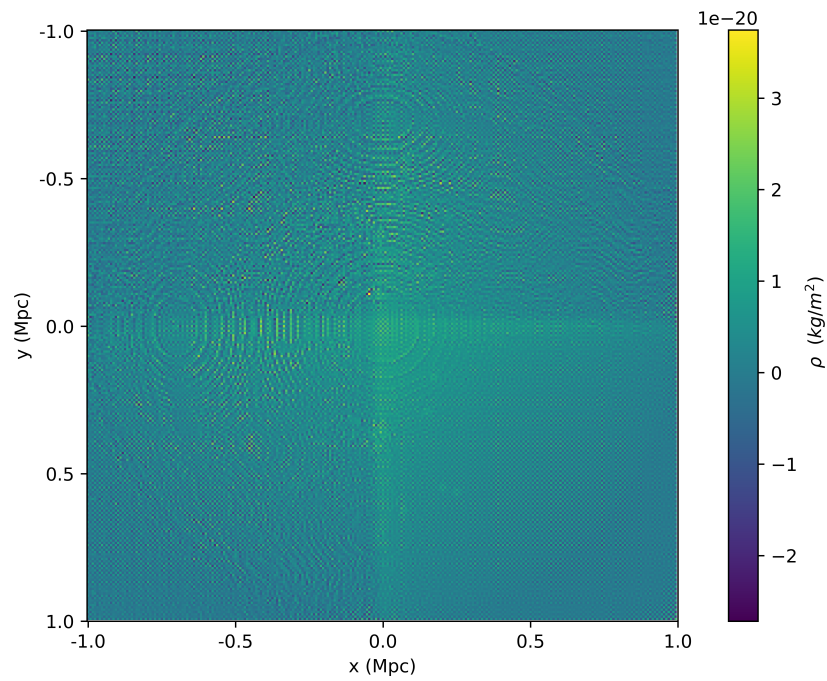


Figure A.3: Apparent matter using MOND with the Verlinde interpolation function.

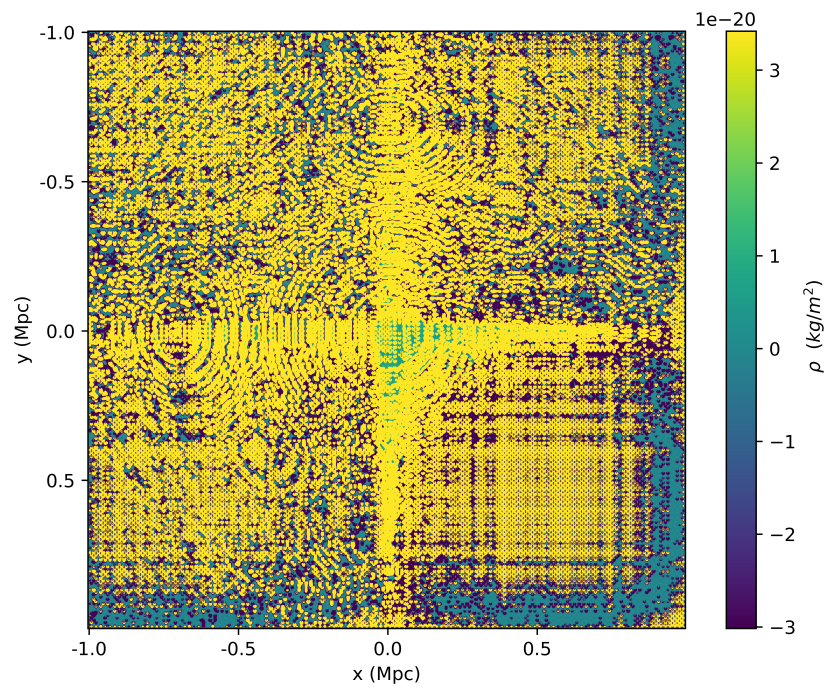


Figure A.4: Apparent dark matter using MOND with the Verlinde interpolation function. The apparent dark matter is obtained by subtracting the baryonic matter from the apparent matter. The black contour correspond to $\Sigma_{\text{apparentDM}} = 2 \cdot 10^{-21}$ and the yellow contours correspond to $\Sigma_{\text{apparentDM}} = 4 \cdot 10^{-21}$.

B

Code

In this section, the code used in this thesis is presented. The code used to create the plots are not included.

First the constants are introduced

```
import numpy as np
import matplotlib.pyplot as plt
from matplotlib import cm
import gc

L = 256 #half the size grid
R = 2000 #radius cluster in kpc

#Constants
ly = 9.4605284 * 10**15 #m Light year
mpc = 3.26 * 10**6 * ly #m Megaparsec
kpc = mpc/1000
M_O = 1.9891*10**30 #kg Solar mass
G = 6.674 * 10**(-11) #m^3/kg/s^2 Gravitational constant
H0 = 72000/mpc # 1/s Hubble constant
a0 = 1.2*10**(-10) #m/s^2
inch = 4.413 #kpc

pixelsize = R/L #kpc per pixel
stepsize = pixelsize*kpc #m per pixel
kstep = np.pi/(R*kpc) #step in k-space

ne0 = 7.2*10**(-3) * 10**6 #number of electrons per m^3
massp = 1.673 * 10**(-27) #mass proton
rhogas = ne0 * massp * (pixelsize*kpc)**3 /M_O #sunmasses/pixel
rhogas2 = ne0 * massp * stepsize**3 #kg/pixel
radiusc = int(np.floor(496.6/pixelsize)) #pixels
radiusc2 = int(np.floor(1000/pixelsize)) #pixels
Mmilkyway = 1.26 * 10**12 * M_O * 0.1 #10 percent baryonic matter

#constants from paraficz et al
vdisp1 = 884.2 * 10**3 #m/s
vdisp2 = 840.2 * 10**3
vdisp3 = 795.7 * 10**3
rcore1 = 117.4 * kpc #m
rcore2 = 127.3 * kpc
```

```

rcore3 = 47.3 * kpc
rcut = 1000 * inch * kpc
xdl1 = [-92* inch * kpc+L*stepsize, -45 * inch * kpc+L*stepsize]
xdl2 = [-75 * inch * kpc+L*stepsize, -15 * inch * kpc+L*stepsize]
xdl3 = [85 * inch * kpc+L*stepsize, 10 * inch * kpc +L*stepsize]

#constants found for the inverse distribution function
inb1 = 6.07 * 10**-4
ina1 = 5.03 * 10**-6
inb2 = 1.14 * 10**-3
ina2 = 7.81 * 10**-6

rho = np.zeros((2*L,2*L,2*L)) #mass density

#reshape indices
reshaped = list(np.arange(L,2*L))
reshaped.extend(list(np.arange(L)))

#initialize k-space
kX = np.arange(-L,L)
kY = np.arange(-L,L)
kZ = np.arange(-L,L)
K3 = np.meshgrid(kX,kY,kZ)
K3L = K3[0]**2 + K3[1]**2 + K3[2]**2
K3L[L,L,L] = 1
K3L = K3L[:, :, reshaped]
K3L = K3L[:, reshaped, :]
K3L = K3L[reshaped, :, :]
K3Linv = 1/K3L

#construct inproduct matrices
inprodx = np.meshgrid(np.zeros(2*L), kX, np.zeros(2*L))
inprodx = inprodx[1]
inprodx = inprodx[:, :, reshaped]
inprodx = inprodx[:, reshaped, :]
inprodx = inprodx[reshaped, :, :]

inprody = np.meshgrid(kY, np.zeros(2*L), np.zeros(2*L))
inprody = inprody[0]
inprody = inprody[:, :, reshaped]
inprody = inprody[:, reshaped, :]
inprody = inprody[reshaped, :, :]

inprodz = np.meshgrid(np.zeros(2*L), np.zeros(2*L), kZ)
inprodz = inprodz[2]
inprodz = inprodz[:, :, reshaped]
inprodz = inprodz[:, reshaped, :]
inprodz = inprodz[reshaped, :, :]

```

Now the functions are defined:

```

def NDpotential(rho): #obtain Newtonian potential
    phi = np.zeros((2*L,2*L,2*L))
    rho_hat = np.fft.fftn(rho)

```

```

f = -4*G*np.pi* rho*hat*K3Lin*V/kstep**2
phi = np.fft.ifftn(f)
return np.real(phi)

def MDconstcirc(r, x0, M): #create uniform circle mass density
    density = M
    norm = 0
    rho = np.zeros((2*L,2*L))
    for i in range(-r,r+1):
        for j in range(-r,r+1):
            if (i**2 + j**2 <= r**2):
                norm += 1
                rho[x0[0]+i,x0[1]+j] = M
    rho = rho/norm
    return rho

def vectorfield(phi): #obtain acceleration field from a potential
    phihat = np.fft.fftn(phi) #obtain fourier transform Newtonian potential
    ghat = np.zeros((3,2*L,2*L,2*L), dtype = 'complex_')
    ghatx = 1j * kstep * phihat*inprodx
    ghaty = 1j * kstep * phihat*inprody
    ghatz = 1j * kstep * phihat*inprodz
    gx = np.fft.ifftn(ghatx)
    gy = np.fft.ifftn(ghaty)
    gz = np.fft.ifftn(ghatz)
    return gx, gy, gz

def divergence(fx, fy, fz): #calculate the divergence of a vector
    fhatx = np.fft.fftn(fx)
    fhaty = np.fft.fftn(fy)
    fhatz = np.fft.fftn(fz)
    ax = np.fft.ifftn(1j * inprodx * kstep * fhatx)
    ay = np.fft.ifftn(1j * inprody * kstep * fhaty)
    az = np.fft.ifftn(1j * inprodz * kstep * fhatz)
    return ax + ay + az

def curl(fx, fy, fz): #calculate the curl of a vector
    fhatx = np.fft.fftn(fx)
    fhaty = np.fft.fftn(fy)
    fhatz = np.fft.fftn(fz)
    ax = np.fft.ifftn(1j * (inprody * kstep * fhatz - inprodz * kstep * fhaty ))
    ay = np.fft.ifftn(1j * (inprodx * kstep * fhatz - inprodx * kstep * fhatz ))
    az = np.fft.ifftn(1j * (inprodx * kstep * fhaty - inprody * kstep * fhatx ))
    return ax, ay, az

def MOND(rho, n, inter): #MOND potential, with n iterative steps and interpolation function
    phi = NDpotential(rho) #obtain newtonian potential
    print("A")
    gx, gy, gz = vectorfield(phi) #obtain acceleration in normal space
    Fx = np.zeros((2*L,2*L,2*L), dtype = 'complex_')
    Fy = np.zeros((2*L,2*L,2*L), dtype = 'complex_')
    Fz = np.zeros((2*L,2*L,2*L), dtype = 'complex_')
    Fx = gx #initialize F
    Fy = gy
    Fz = gz

```

```

del phi
gc.collect() #free up memory
fx, fy, fz = inverse(Fx, Fy, Fz, inter) #inverse interpolation function
print("B")
for i in range(n): #start iterative process
    fparx, fpary, fparz = f_it(fx, fy, fz) #find parrallel component
    Fx, Fy, Fz = interpolation(fparx, fpary, fparz, inter) #interpolation function
    print("C")
    Bx = Fx - gx #start with B
    By = Fy - gy
    Bz = Fz - gz
    del Fx, Fy, Fz
    Bx, By, Bz = B_it(Bx, By, Bz) #find perpendicular component
    print("D")
    Fx = gx + Bx #initialize F
    Fy = gy + By
    Fz = gz + Bz
    fx, fy, fz = inverse(Fx, Fy, Fz, inter)
del Fx, Fy, Fz
gc.collect()
fhatx = np.fft.fftn(fx)
fhaty = np.fft.fftn(fy)
fhatz = np.fft.fftn(fz)
print("E")
phidhat = np.zeros((2*L,2*L,2*L), dtype = 'complex_')
phidhat = -1j / kstep * (fhatx*inprodx + fhaty*inprody + fhatz*inprodz) * K3Linv #calculate
phid = np.real(np.fft.ifftn(phidhat))
return phid

def f_it(fx, fy, fz): #finding the component parrallel to the wave vector k
    fhatx = np.fft.fftn(fx)
    fhaty = np.fft.fftn(fy)
    fhatz = np.fft.fftn(fz)
    num = np.zeros((2*L,2*L,2*L), dtype = 'complex')
    num = fhatx*inprodx + fhaty*inprody + fhatz*inprodz
    fhatparx = inprodx*num*K3Linv
    fhatpary = inprody*num*K3Linv
    fhatparz = inprodz*num*K3Linv
    fparx = np.fft.ifftn(fhatparx)
    fpary = np.fft.ifftn(fhatpary)
    fparz = np.fft.ifftn(fhatparz)
    return fparx, fpary, fparz

def B_it(Bx, By, Bz): #finding the component perpendicular to the wave vector k
    Bhatx = np.fft.fftn(Bx)
    Bhaty = np.fft.fftn(By)
    Bhatz = np.fft.fftn(Bz)
    num = np.zeros((2*L,2*L,2*L), dtype = 'complex')
    num = Bhatx*inprodx + Bhaty*inprody + Bhatz*inprodz
    Bhatperx = Bhatx-num*inprodx*K3Linv
    Bhatpery = Bhaty-num*inprody*K3Linv
    Bhatperz = Bhatz-num*inprodz*K3Linv
    Bx = np.fft.ifftn(Bhatperx)
    By = np.fft.ifftn(Bhatpery)
    Bz = np.fft.ifftn(Bhatperz)
    return Bx, By, Bz

```

```

def interpolation(x, y, z, inter): #all interpolation functions and also deep mond
    mux = np.zeros((2*L,2*L,2*L), dtype = 'complex')
    muy = np.zeros((2*L,2*L,2*L), dtype = 'complex')
    muz = np.zeros((2*L,2*L,2*L), dtype = 'complex')
    xnorm = np.zeros((2*L,2*L,2*L), dtype = 'complex')
    if (inter==0): #deepmond
        xnorm = np.sqrt(x**2+y**2+z**2) / a0
        mux = xnorm * x
        muy = xnorm * y
        muz = xnorm * z
    if (inter==1): #standard
        xnorm = np.sqrt(x**2+y**2+z**2) / a0
        mux = xnorm/np.sqrt(1+xnorm**2)*x
        muy = xnorm/np.sqrt(1+xnorm**2)*y
        muz = xnorm/np.sqrt(1+xnorm**2)*z
    if (inter==2): #verlinde
        xnorm = np.sqrt(x**2+y**2+z**2) / a0
        mux = (np.sqrt(1+4*xnorm) - 1)**2 / (4*xnorm) * x
        muy = (np.sqrt(1+4*xnorm) - 1)**2 / (4*xnorm) * y
        muz = (np.sqrt(1+4*xnorm) - 1)**2 / (4*xnorm) * z
    if (inter==3): #angus
        xnorm = np.sqrt(x**2+y**2+z**2) / a0
        mux = xnorm/(1+xnorm) * x
        muy = xnorm/(1+xnorm) * y
        muz = xnorm/(1+xnorm) * z
    return mux, muy, muz

```

```

def inverse(x,y,z, inter): #all inverse interpolation functions and deep mond
    mux = np.zeros((2*L,2*L,2*L), dtype = 'complex')
    muy = np.zeros((2*L,2*L,2*L), dtype = 'complex')
    muz = np.zeros((2*L,2*L,2*L), dtype = 'complex')
    if (inter==0): #Deep MOND
        xL = np.sqrt(x**2+y**2+z**2)
        xnorm = np.sqrt(a0/xL)
        np.nan_to_num(xnorm)
        mux = xnorm*x
        muy = xnorm*y
        muz = xnorm*z
    if (inter==1): #standard
        xnorm = np.sqrt(x**2+y**2+z**2)
        mux = np.sqrt(1/2 + 1/2*np.sqrt(1+4*a0**2/xnorm**2))*x
        muy = np.sqrt(1/2 + 1/2*np.sqrt(1+4*a0**2/xnorm**2))*y
        muz = np.sqrt(1/2 + 1/2*np.sqrt(1+4*a0**2/xnorm**2))*z
    if (inter==2): #Verlinde
        mux = x + np.emath.sqrt(a0*x)
        muy = y + np.emath.sqrt(a0*y)
        muz = z + np.emath.sqrt(a0*z)
    if (inter==3): #angus
        xnorm = np.sqrt(x**2+y**2+z**2)
        mux = (1/2+1/2*np.sqrt(1+4*a0/xnorm))*x
        muy = (1/2+1/2*np.sqrt(1+4*a0/xnorm))*y
        muz = (1/2+1/2*np.sqrt(1+4*a0/xnorm))*z
    return mux, muy, muz

```

```

def sigma_dPIE(rcore , rcut, x0, s0): #projected mass distribution for the dPIEmds, thus the dark matter

```

```

sigma = np.zeros((2*L,2*L))
for i in range(0,2*L):
    for j in range(0,2*L):
        R = (x0[0]-i*stepsize)**2+(x0[1]-j*stepsize)**2
        sigma[i, j] = s0**2*rcut/(2*G*(rcut-rcore))*((1/np.sqrt(rcore**2+R))-(1/np.sqrt(r
return sigma

def randomize(): #bullet cluster simulation with n galaxies
rho = np.zeros((2*L,2*L,2*L))
theta = []
phi = []
r = []
for i in range(40):
    u = np.random.uniform()
    v = np.random.uniform()
    theta.append(np.pi * 2 * u)
    phi.append(np.arccos(2*v-1))

for i in range(25): #randomized around -370, -130 kpc
    y = np.random.uniform()
    r.append(int(invradial1(y)/pixelsize))
    coordsx = int(r[i]*np.sin(theta[i])*np.cos(phi[i]))
    coordsy = int(r[i]*np.sin(theta[i])*np.sin(phi[i]))
    coordsz = int(r[i]*np.cos(theta[i]))
    rho[:, :, L+coordsz] += MDconstcirc(round(16.3/pixelsize), [L+coordsx-int(370/pixelsize), L+
#[L+coordsx-int(370/pixelsize), L+coordsy-int(130/pixelsize), L+coordsz] = Mmilkyway/stepsi

for i in range(15): #randomized around 370, 40 kpc
    y = np.random.uniform()
    r.append(int(invradial2(y)/pixelsize))
    coordsx = int(r[i]*np.sin(theta[i])*np.cos(phi[i]))
    coordsy = int(r[i]*np.sin(theta[i])*np.sin(phi[i]))
    coordsz = int(r[i]*np.cos(theta[i]))
    rho[:, :, L+coordsz] += MDconstcirc(round(16.3/pixelsize), [L+coordsx+int(370/pixelsize), L+
#[L+coordsx+int(370/pixelsize), L+coordsy+int(40/pixelsize), L+coordsz] = Mmilkyway/stepsi
return rho

def invradial1(w): #inverse radial cumulative distribution function for the main cluster
return np.sqrt(inb1**2/(4*ina1**2)+w/ina1)-inb1/(2*ina1)

def invradial2(w): #inverse radial cumulative distribution function for the sub cluster
return np.sqrt(inb2**2/(4*ina2**2)+w/ina2)-inb2/(2*ina2)

def projection(rho): #project 3D mass density to 2D projected mass density
sigma = np.zeros((2*L,2*L))
sigma = np.sum(rho, axis=2)
return sigma

def apparentmatter(phi): #find apparent matter from potential, assuming ND
phihat = np.fft.fftn(phi)
rho_hat = - kstep**2 * K3L * phihat/(4 * np.pi * G)
rho = np.real(np.fft.ifftn(rho_hat))
return rho

```

Mass generation:

```
#initialize all the masses

#MOND model
intracluster = np.zeros((2*L,2*L,2*L)) #gas is put in the middle
for i in range(-radiusc2,radiusc2+1):
    for j in range(-radiusc2,radiusc2+1):
        for k in range(-radiusc2,radiusc2+1):
            if (i**2 + j**2 + k**2 < radiusc2**2):
                intracluster[L+i,L+j,L+k] = 2 * rhogas2 *(1+ ((i)**2+(j)**2+(k)**2)/radiusc**2)**(-1)/

galaxies = randomize()
baryonicmass = galaxies + intracluster

#dark matter model
massDM1 = sigma_dPIE(rcore1,rcut,xdm1,vdisp1)
massDM2 = sigma_dPIE(rcore2,rcut,xdm2,vdisp2)
massDM3 = sigma_dPIE(rcore3,rcut,xdm3,vdisp3)
sigma_DM = massDM1 + massDM2 + massDM3
```